REPORT DOCUMENTATION PAGE

1. REPORT DATE *(DD-MM-YYYY)*
10/Aug/2001

2. REPORT TYPE
THESIS

3. DATES COVERED *(From - To)*

4. TITLE AND SUBTITLE
DESIGN AND TESTING OF A HYDROGEN PEROXIDE MICRO ELECTROMECHANICAL SYSTEMS THRUSTER

5a. CONTRACT NUMBER

5b. GRANT NUMBER

5c. PROGRAM ELEMENT NUMBER

6. AUTHOR(S)
2D LT THOMAS MICHAEL A

5d. PROJECT NUMBER

5e. TASK NUMBER

5f. WORK UNIT NUMBER

7. PERFORMING ORGANIZATION NAME(S) AND ADDRESS(ES)
GEORGE WASHINGTON UNIVERSITY

8. PERFORMING ORGANIZATION REPORT NUMBER
CI01-198

9. SPONSORING/MONITORING AGENCY NAME(S) AND ADDRESS(ES)
THE DEPARTMENT OF THE AIR FORCE
AFIT/CIA, BLDG 125
2950 P STREET
WPAFB OH 45433

10. SPONSOR/MONITOR'S ACRONYM(S)

11. SPONSOR/MONITOR'S REPORT NUMBER(S)

12. DISTRIBUTION/AVAILABILITY STATEMENT
Unlimited distribution
In Accordance With AFI 35-205/AFIT Sup 1

13. SUPPLEMENTARY NOTES

14. ABSTRACT

20010904 029

15. SUBJECT TERMS

16. SECURITY CLASSIFICATION OF:

a. REPORT	b. ABSTRACT	c. THIS PAGE

17. LIMITATION OF ABSTRACT

18. NUMBER OF PAGES
104

19a. NAME OF RESPONSIBLE PERSON

19b. TELEPHONE NUMBER *(Include area code)*

Author: Michael A. Thomas, Second Lieutenant, United States Air Force
Title: "Design and Testing of a Hydrogen Peroxide Microelectromechanical Systems
    Thruster"
Year: 2000
Pages: 104
Degree: Master of Science in Aerospace Engineering
Institution: George Washington University

Abstract:

Microelectromechanical Systems (MEMS) fabrication techniques were used to build miniature thrusters from a silicon wafer, drastically reducing the size and volume from conventional techniques. These thrusters incorporate a catalyst within the wafer and are therefore reusable. This project was the first known effort to develop catalytic MEMS thrusters. 85-90% hydrogen peroxide was studied and used as a monopropellant in the thruster design due to its safety advantages over other propellants and the renewed interest in the scientific community. This research effort formulated concepts, performed analysis, and developed fabrication techniques to construct and test a prototype thruster in order to develop the proof-of-concept fundamentals needed for a MEMS monopropellant thruster.

Several thruster concepts of varying catalyst and nozzle sizes were designed in order to determine appropriate scaling laws. The estimated thrust level range was between 100 and 400 μN with impulse bits between 1-1000 uN·sec and a specific impulse of approximately 140 seconds. Individual reaction chambers are approximately 3x2.5x 0.5 mm. Thrust chambers were etched in a 0.5 mm silicon substrate and vapor deposited with titanium and silver using a shadow mask. The chamber fabrication process was completed by anodically bonding glass to the substrate; cutting each chamber from the wafer with a diamond saw, and integrating propellant feed tubes. Reaction tests validate that high decomposition efficiencies can be obtained with residence times greater than 0.6 seconds, corresponding to catalyst lengths of 3-4mm. Included in this research was an investigation into the special requirements needed for storage, handling and operation of high-test hydrogen peroxide.

Bibliography:

1.   H. McCurdy, *Inside NASA*, Johns Hopkins University Press, 1993.
2.   D. Goldin, Remarks at the FY2001 Budget Press Conference, 7 February 2000.
3.   J. Pollard, C. Chao, and S. Janson, "Populating and Maintaining Cluster Constellations in Low-Earth Orbit," Proceedings of the 35th AIAA/ASME/SAE/ASEE Joint Propulsion Conference & Exhibit, Los Angeles, CA, June 1999.
4.   "Pint-Size Satellites Will Soon Be Doing Giant Jobs," Business Week Online, http://design.caltech.edu/micropropulsion/business_week/index.html, Accessed on 25 May 2000.
5.   H. Helvajian, editor, *Microengineering Aerospace Systems*, ISBN 1-884989-03-9, Aerospace Press, El Segundo CA, and AIAA, Reston VA 1999.
6.   "MEMS Microthruster Propulsion System," http://www.darpa.mil/MTO/MEMS/Projects/individual_53.html. Accessed on 13 October 2000.
7.   "Advanced Propulsion Concepts: Micro-thrusters", http://sec353.jpl.nasa.gov/apc/Micropropulsion/01.html Accessed on 18 January 2000.

8. W. Janson and Henry Helvajian, "MEMS, Microengineering, and Aerospace Systems," AIAA 99-3802.

9. M. Zaghoul, "Military Applications of MEMS," George Washington University, http://www.arpa.mil/mto/mems/projects/individual_25.html.

10. S. Janson, H. Helvajian, W. Hansen, and J. Lodmell, "Batch-Fabricated CW Microthrusters for Kilogram-Class Spacecraft," AIAA 99-2722, Proceedings of the 35th AIAA/ASME/SAE/ASEE Joint Propulsion Conference & Exhibit, Los Angeles, CA, June 1999.

11. R.L. Bayt, A.A. Ayon, and K.S. Breuer, "A Performance Evaluation of MEMS-based Micronozzles," AIAA 97-3169, Proceedings of the 33rd AIAA/ASME/SAE/ASEE Joint Propulsion Conference and Exhibit, Seattle WA, July 1997.

12. B. Reed, "Micropropulsion Activities at NASA Lewis Research Center," Proceedings of the Joint AFRL/MIT Formation Flying and Micro Propulsion Workshop, Oct 1998.

13. E. Antonsson and S.W. Janson, "MEMS Microthruster Digital Propulsion System," Proceedings of the Joint AFRL/MIT Formation Flying and Micro Propulsion Workshop, Oct 1998.

14. D. Lewis, S. Janson, and R. Cohen, "Digital Micro-Propulsion Project," Sensors and Actuators A, 2000. pp. 143-154.

15. G. Spanjers, "Micro-Propulsion Research at Air Force Research Laboratory," Proceedings of the Joint AFRL/MIT Formation Flying and Micro Propulsion Workshop, Oct 1998.

16. C. Zakrzwski, NASA GSFC Propulsion Branch. Private Communication, 2000.

17. M. Giulio, "Design of a Highly Integrated Micropropulsion System for Microsatellites Attitude Control," Proceedings of the 36th AIAA/ASME/SAE/ASEE Joint Propulsion Conference & Exhibit, Huntsville, AL, July 2000.

18. E. Wernimont and P. Mullens, "Capabilities of Hydrogen Peroxide Catalyst Beds," Proceedings of the 36th AIAA/ASME/SAE/ASEE Joint Propulsion Conference & Exhibit, Huntsville, AL, July 2000.

19. "Hazards of Chemical Rockets and Propellants," Chemical Propulsion Information Agency Publication 394, Volume III, Sept 1984.

20. M. Jeff, "Hydrogen Peroxide-The Safe Supply and Handling of HTP," Proceedings of the 1st Annual Hydrogen Peroxide Conference, Surrey U.K. 1998.

21. J.J. Rusek and N.M Anderson, "Heterogeneous Decomposition of Rocket Grade Hydrogen Peroxide," Proceedings of the 1st Annual Hydrogen Peroxide Conference, Surrey, UK, 1998.

22. H.N. Feigenbaum, N. Nimmerfroh, and E. Walzer, "Practical Experiences with High Test Hydrogen Peroxide," Proceedings of the 28th Propellant Development and Characterization Subcommittee and 17th Safety and Environmental Protection Subcommittee Joint Meeting, April 1999.

23. J.C. Whitehead, "Hydrogen Peroxide Propulsion for Smaller Satellites," Proceedings of the 12th AIAA/USU Conference on Small Satellites, SSC98-VIII-1.

24. D. Pauls and S. McMahon, "Transportation, Storage and Handling of PROPULSE™ HTP," Proceedings of the 2nd International Hydrogen Peroxide Conference, Nov 1999.

25. J.C. Whitehead, "Hydrogen Peroxide Propulsion for Smaller Satellites," Proceedings of the 12th AIAA/USU Conference on Small Satellites, SSC98-VIII-1.

26. 25. M.K. Minthorn, "Future Navy Missile Propulsion Needs," Proceedings of the 2nd International Hydrogen Peroxide Conference, Nov 1999.

27. E.J. Wernimott, M. Ventura, G. Garboden, and P. Muellens, "Past and Present Uses of Rocket Grade Hydrogen Peroxide," Proceedings of the 2nd International Hydrogen Peroxide Conference, Nov 1999.

28. "TSRS MSDS Number 08193," http://msds.ksc.nsaa.gov/msds/08192.html Accessed on 5 February 2000.

29. J. McCormick, "Hydrogen Peroxide Rocket Manual," FMC Corporation.

30. "Hydrogen Peroxide for Rocket Propulsion Applications," J. Rusek, Chemical Propulsion Information Agency Publication 630, Volume I, Dec 1995.

31. "Hazards of Chemical Rockets and Propellants," Chemical Propulsion Information Agency Publication 394, Volume III, Sept 1984.

32.   J.C. Whitehead, "Progress Towards Hydrogen Peroxide," Proceedings of the 13th AIAA/USU Conference on Small Satellites, SSC98-XII-5.

33.   Chemical Propulsion Information Agency, Liquid Propellant Manual, September 1997.

34.   N. Nimmerfroh, H. Feigenbaum, and E. Walzer, "PROPULSE™ Hydrogen Peroxide: History, Manufacture, Quality, and Toxicity," Proceedings of the 2nd International Hydrogen Peroxide Conference, Nov 1999.

35.   D.R. Mattie, "Toxicity of Rocket Fuels: Comparison of Hydrogen Peroxide with Current Propellants," Proceedings of the 1st Annual Hydrogen Peroxide Conference, Surrey, UK, 1998.

36.   E.J. Wernimott, M. Ventura, G. Garboden, and P. Muellens, "Past and Present Uses of Rocket Grade Hydrogen Peroxide," Proceedings of the 2nd International Hydrogen Peroxide Conference, Nov 1999.

37.   M.K. Minthorn, "Future Navy Missile Propulsion Needs," Proceedings of the 2nd International Hydrogen Peroxide Conference, Nov 1999.

38.   Proceedings of the 2nd International Hydrogen Peroxide Conference, Nov 1999.

39.   J. Mueller, J. Bellan, F. Noca, and I. Chakraborty, "Feasibility Investigation of a Microfabricated Vaporizing Liquid Micro-Thruster," JPL Proposal , 21 January 1999.

40.   "Catalysis," http://www.chem.ualberta.ca/~plambeck/che/p102/p02173 Accessed on 8 April 2000.

41.   R. Eloirdi, S. Rossignol,M. Chauveau,C. Kappenstein, and D. Duprez, "Design and Use of a Batch Reactor for Catalytic Decomposition of Different Monopropellants," Proceedings of the 36th AIAA/ASME/SAE/ASEE Joint Propulsion Conference & Exhibit, Huntsville, AL, July 2000.

42.   J.J. Sellers, R. Brown, and M. Paul, "Practical Experience with Hydrogen Peroxide Catalysts," Proceedings of the 1st Annual Hydrogen Peroxide Conference, Surrey, UK, 1998.

43.   J. Rusek, Professor at Purdue University. Private Communication, Oct 1999.

44.   M. Bettner and R. Humble, "Polyethylene and Hydrogen Peroxide Hybrid Testing at the United States Air Force Academy," Proceedings of the 1st Annual Hydrogen Peroxide Conference, Surrey U.K. 1998.

45.   W. Janson and Henry Helvajian, "MEMS, Microengineering, and Aerospace Systems," AIAA paper 99-3802, 1999.

46.   R.L. Bayt, A.A. Ayon, and K.S. Breuer, "A Performance Evaluation of MEMS-based Micronozzles," Proceedings of the 33rd AIAA/ASME/SAE/ASEE Joint Propulsion Conference and Exhibit, Seattle WA, July 1997, AIAA paper 97-3169.

47.   P.V. Panetta, "NASA-GSFC Nano-Satellite Technology Development," Proceeding of the 12th AIAA/USU Conference on Small Satellites, SSC98-VI-5.

48.   "Advanced Propulsion Concepts: Micro-Thrusters," http://sec353.jpl.nasa.gov/apc/Micropropulsion/01.html. Accessed on 18 January 2000.

49.   B. Mott, NASA GSFC Detector Systems Branch. Private Communication, Jan 2000.

50.   J. Whitehead, "Hydrogen Peroxide Storage in Small Sealed Tanks," Proceedings of the 2nd International Hydrogen Peroxide Conference, Nov 1999.

51.   D. Hitt, University of Vermont. Private Communication, Aug 2000.

52.   R. Humble, *Space Propulsion Analysis and Design*, McGraw-Hill. 1995.

53.   D. Willis, NASA GSFC Propulsion Branch. Private Communication, Oct 2000.

Design and Testing of a Hydrogen Peroxide Microelectromechanical Systems Thruster

By

2nd Lieutenant Michael A. Thomas

B.S. June, 1999, United States Air Force Academy

A Thesis submitted to

The Faculty of

The School of Engineering and Applied Science
of the George Washington University in partial satisfaction
of the requirements for the degree of Master of Science

20 December 2000

Thesis directed by

Catherine Mavriplis

Professor of Engineering and Applied Science

ABSTRACT

Microelectromechanical Systems (MEMS) fabrication techniques were used to build miniature thrusters from a silicon wafer, drastically reducing the size and volume from conventional techniques. These thrusters incorporate a catalyst within the wafer and are therefore reusable. This project was the first known effort to develop catalytic MEMS thrusters. 85-90% hydrogen peroxide was studied and used as a monopropellant in the thruster design due to its safety advantages over other propellants and the renewed interest in the scientific community. This research effort formulated concepts, performed analysis, and developed fabrication techniques to construct and test a prototype thruster in order to develop the proof-of-concept fundamentals needed for a MEMS monopropellant thruster.

Several thruster concepts of varying catalyst and nozzle sizes were designed in order to determine appropriate scaling laws. The estimated thrust level range was between 100 and 400 μN with impulse bits between 1-1000 uN·sec and a specific impulse of approximately 140 seconds. Thrust-to-weight ratios were on the order of 1.8. Individual reaction chambers are approximately 3x2.5x 0.5 mm. Thrust chambers were etched in a 0.5 mm silicon substrate and vapor deposited with titanium and silver using a shadow mask. The chamber fabrication process was completed by anodically bonding glass to the substrate, cutting each chamber from the wafer with a diamond saw, and integrating propellant feed tubes. Reaction tests validate that high decomposition efficiencies can be obtained with residence times greater than 0.6 seconds, corresponding to catalyst lengths of 3-4mm. Included in this research was an investigation into the special requirements needed for storage, handling and operation of high-test hydrogen peroxide. When compared to other proposed micro-propulsion concepts, MEMS catalytic monopropellant thrusters show the promise of the combined advantages of high specific density, low system power and volume, large range of thrust levels, repeatable thrust vectors, and simplicity of integration and control.

Acknowledgements

CONTENTS

LIST OF EQUATIONS

LIST OF FIGURES

LIST OF TABLES

LIST OF SYMBOLS

A: Cross-Sectional Area
Acat: Catalyst Frontal Area
$Acat_{min}$: Minimum Catalyst Frontal Area to Meet Flux requirements
A_e: Nozzle Exit Area
A_{inj}: Injector Area
A_t: Nozzle Throat Area
c^*:   Characteristic Velocity
Ca: Concentration
Ca_0:   Initial Concentration
C_f: Coefficient of Thrust
D_e: Diameter of Nozzle Exit
D_{cat}: Catalyst Frontal Diameter
D_t: Nozzle Throat Diameter
F: Thrust
g_0:   Gravitational Constant
H: Characteristic Scale Length
ISP: Specific Impulse
ISP_{eff}: Specific Impulse Efficiency
K: Head Loss Coefficient-or-Thermal Conductivity
Kn: Knudsen Number
l: Mean Free Path
M: Mach Number
Mdot: Mass Flow Rate
$Mdot_{eff}$: Mass Flow Rate Efficiency
M_e: Exit Mach Number
MW: Molecular Weight
ΔP: Pressure Drop
P_0:   Chamber Pressure
P_a: Atmospheric Pressure
P_e: Exit Pressure
q: Heat
R: Universal Gas Constant
Re: Reynolds Number
t: Time
ΔT: Temperature Differential
T: Local Temperature
T_c: Chamber Temperature
$Thrust_{corr}$: Thrust Corrected for Efficiencies
U: Velocity
y: Distance From wall
γ: Ratio of Specific Heats
ε: Emmissivity
μ: Coefficient of Viscosity
ρ: Density
σ: Coefficient of Tangential Momentum Accommodation-or-Stefan-Boltzmann Constant

1. Introduction

1.1 The Need for Micropropulsion

With the maxim "Faster, Better, Cheaper," NASA, the Department of Defense (DOD) and the aerospace community enter a new millennium searching for ways to improve efficiency and end the need for large multibillion dollar spacecraft. As the budget-friendly space race has been forgotten and the Cold War threat is gone, the seemingly unlimited budget for space activities has now been restricted to a point where new approaches must be found to continue meaningful space initiatives at a lower cost. In Fiscal Year 1965, NASA had 4.4% of the total Federal budget[1], while the budget in Fiscal Year 1999[2] gives it less than 1%, the smallest budget of any of the major agencies in the Federal government.

This noteworthy trend is not restricted to NASA and is just one example that is forcing a paradigm shift across all of government, industry, and academia. A harbinger of this new period of thought is the introduction and increased emphasis on microspacecraft. Smaller mass and volume indicate lowered launch costs as multiple spacecraft can be launched on a single launch vehicle or smaller launch vehicles can be utilized. Many performance-related attributes also improve at the smaller scale. The main advantage comes from the cubed-squared law,

which states that properties that are a function of volume (such as mass) decrease faster than those that are a function of area (such as thrust). The outcome is that better thrust-to-weight ratios can be expected on smaller scale spacecraft, yielding smaller propellant requirements.

This push for nanosatellites is also coupled to a second trend in the aerospace community as well, distributed space formations, or formation flying. Distributed spacecraft allow multiple spacecraft to act together as a much larger sensor, without the complexity or cost of a larger platform. One such concept is described below. Each satellite would have a slightly different inclination, causing the satellites to "orbit" around a center mother satellite. Figure 1 illustrates this principle. Each satellite could contain a different sensor (or a redundant sensor) with all of the information relayed to the ground. A singular satellite failure would then no longer devastate the mission. It is necessary to know the exact position of the nanosatellites as well as have the ability to accurately move them to a scale never previously needed in order to accomplish this very complex feat.
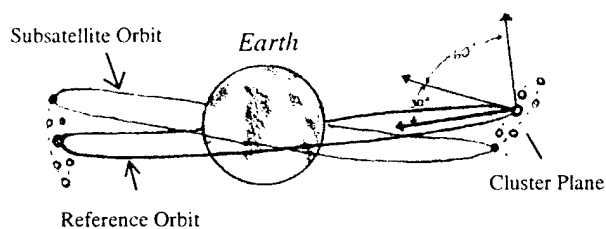
Figure 1. Formation Flying Concept: Subsatellite in tilted orbit executes cyclic motion in reference to center satellite and returns to initial position after one revolution.[3]

The potential for these nanosatellites is creating excitement across the military and commercial sectors. As an example, the Clinton Administration increased nanotechnology funding 84% in his 2001 budget request. The development of micro-systems specifically will get a 57% budgetary increase within the DOD.[4]

While some nanosatellites are simply smaller scale versions of their larger predecessors, most require completely new paradigms of thought, as many of the assumptions taken for granted in larger systems are no longer valid. This problem is seen most clearly in the development of propulsion systems for these satellites. With the total satellite mass decreasing, the dimensional size of the already small propulsion system must decrease as well. Envisioning satellites the size of softballs, equivalent propulsion systems must be on the micron scale. Manufacturing these systems becomes the critical challenge. Additionally, if fluid propellants are utilized, the fluid mechanics at this level transcends traditional work. Viscous

losses, usually neglected in larger scale thrusters, play a vital role in nano-thrusters and could greatly diminish the thrust output.

Still a relatively new field, only truly enabled within the past decade, the specific classifications of small-scale satellites are still in a state of flux. Only a decade ago, the smallest satellite thought feasible was a microsatellite, which NASA defined as any satellite under 100kg. Now, many micro engineering experts such as Helvajian have divided satellite technology many times further into nanosatellites ($\approx$1g-1kg mass), picosatellites ($\approx$1mg-1g mass) and femtosatellites ($\approx$1μg-1mg mass)[5]. For the sake of clarity and brevity in this paper, any satellite falling into any of the aforementioned categories will be termed a nanosatellite.

1.2 Microelectromechanical Systems

The general requirements for a nanosatellite propulsion system are small mass($<$0.1kg), volume($<$1cm^3), and impulse bits(1-1000μNs), while being easily reproducible. No current technology meets these requirements. Fabrication of such devices on the micron and sub-micron level cannot be done with the standard techniques applicable to larger systems. One solution to this problem is to use microelectromechanical systems (MEMS)

4

fabrication techniques to produce thrusters capable of micro-Newton thrust levels. MEMS technology can be used to build an entire system into a silicon microchip, much like an integrated circuit. In a MEMS propulsion system, the pumps, plumbing, sensors, and actuators could theoretically all be etched into a silicon substrate.

The potential advantages of developing a MEMS propulsion system are numerous. They can be extremely small, with dimensions on the micron scale and even smaller depending on the etching technique, which is continuously evolving. They can also be extremely lightweight, have a low cost per device, have very little dead volume, and can be reproduced in mass quantities. In addition, they may be constructed of simple components, some concepts having no moving parts in the thruster itself.

The field of using MEMS for space applications, while nearly non-existent a decade ago, is rapidly increasing as the technology has enabled the full benefits to be realized. Currently, the United States Air Force Research Lab (USAFRL) in Albuquerque, New Mexico is testing MEMS devices' resistance to radiation in support of future MEMS propulsion applications[5,6]. Meanwhile, technology demonstrators are being built by NASA Jet Propulsion Laboratory(JPL)[7] and The Aerospace Corporation[8], while several universities such as the George Washington University

and the Massachusetts Institute of Technology (MIT) are becoming heavily involved in research in the field as well[9,8]. One of the more notable advances is the Defense Advanced Research Projects Agency (DARPA) "digital microthruster," a MEMS based thruster using lead styphnate as the solid propellant[10]. These devices are single shot thrusters with the lead styphnate contained within miniature cavities etched in the silicon. Miniature resistors are attached to one end with a nozzle at the other. A voltage is applied across the resistors to ignite the lead styphnate, which then expands and is expelled through the nozzle.
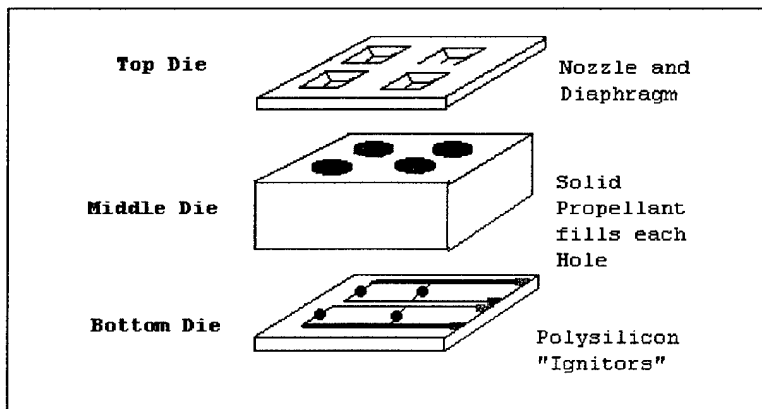
Figure 2. Digital Microthruster Concept[10]

Other significant concepts being pursued include: cold gas systems at MIT[8,11], and the Aerospace Corporation[8]; arrays of solid and bipropellant "digital" single shot thrusters at NASA Glenn Research Center (GRC)[12], and TRW[13,14]; pumped bi-propellant engines at MIT[8,11] and NASA/GRC[12]; resisto-jets being developed at

The Aerospace Corporation[10] and AFRL[15]; and vaporizing liquid and subliming solid thrusters at JPL[7].

While numerous papers on the topic have mentioned the potential of using liquid propellants in a similar manner, little has been done in pursuit of this option. Initial work has been done on bipropellant systems and vaporizing liquid systems, but no one to date has designed or built a catalytic MEMS thruster. In this concept, a propellant tank would pump liquid propellant into the MEMS device and through a catalyst. The propellant would decompose, expand and then exit through a micronozzle, providing a very small and precise impulse bit. The primary advantage of a liquid fueled system is that the thrust vectors would be repeatable, unlike single-shot solid devices, and the operational life would be proportional to the size of the independent propellant tank. Also, the impulse bit from the system is variable with a valve controlling propellant flow duration, allowing for the thrusters to be used for a highly varying range of activities from attitude control to small orbital maneuvers. Having the propellant in high specific density liquid form is also very advantageous over a cold gas system, which occupies a very high volume and requires heavy tanks.

For a number of applications, a working MEMS monopropellant thruster would have an advantage over most current technologies.

They have substantially higher propellant densities and higher specific impulses than cold gas thrusters and greater range of total impulse, thrust level, and impulse bit than discrete solid or bipropellant concepts. They also have simpler actuation design, fixed thrust vectors, and are simpler than bi-propellant systems in both fabrication and propellant handling. Finally, they have lower power requirements than electrothermal devices. For example, resistojets requiring 2 Watts or greater may not be suitable for nanosatellites with 5 Watts or less of total power[16].

While several types of thrusters have their own specific niche within the realm of mission needs, the monopropellant MEMS thruster may be the most flexible. It can serve several propulsion roles and eliminate the need for different propulsion systems onboard a single spacecraft.

1.3 Introduction to MEMS Fabrication

The process by which MEMS devices are created is complex. However, it is important to get a general understanding of the process before a true design can be initiated.

As previously mentioned, the process closely follows the steps involved in the fabrication of an integrated circuit. First, a substrate is selected depending on the specific need of the project. This is usually, while not limited to, silicon.

Section 2.5 will revisit this decision. Crystals of this material are then grown in boules, which are then sliced into wafers and polished. A thin film is then deposited on this wafer. The material used for this film is wide-ranging, depending on the specific application of the system. A design mask is then created. The mask is usually initiated in a CAD software package from which an actual size mask set can be created. Next, a photoresist is used to transfer the pattern of the mask onto the film. The film is then etched away, leaving only the desired pattern on the silicon wafer. This process can be repeated as many times as necessary to create a multi-dimensional system on a wafer.

There are many possible methods for etching as well. Etching techniques can be categorized as either wet or dry. Wet etching involves using a liquid reactant to remove the undesired film. Though the easiest method, it is limited to larger scale MEMS devices. Wet etching techniques usually leave poor definition on deeper etches and tend to round off the edges, problems not inherent in dry etching techniques. Additionally, recent governmental regulations on safety and waste make it a more complex process to handle[5].

In the realm of dry etching techniques, laser 3D ablation and Deep Reactive Ion Etching (DRIE) are two of the newer procedures and produce some of the best results[17]. While

allowing for very fine etching with great definition, both

systems are very expensive and limited to few facilities in

operation. Cooperation with the Detector Systems Branch at NASA

GSFC however, allowed access to their DRIE etching facilities

and thus this method was used in this research. This process

will be described in detail in Chapter 4.

2. Propellant

2.1 Options

In order to develop a monopropellant MEMS thruster, a suitable propellant must first be found. The number of proven monopropellants used in liquid systems is very limited. The only three ever successfully used in flight vehicles are hydrazine, hydrogen peroxide, and propyl nitrate[5]. New "green" monopropellants still under development were not considered for this work. Propyl nitrate is very shock sensitive and is typically used only as a starter fuel. Hydrazine is used in most current systems and has the highest specific impulse. However, recent innovations are allowing the performance of hydrogen peroxide to increase. Meanwhile, its lower toxicity is increasingly more important since minimizing personal and spacecraft risk is becoming more essential. It also has a higher density specific impulse than hydrazine[18], an advantageous characteristic when working with volume constrained systems such as microthrusters. For this effort, high-test (concentrations above 85%) hydrogen peroxide (HTP) was chosen because of its low toxicity and the overall renewed interest.

2.2 Hydrogen Peroxide General Properties

Hydrogen Peroxide is a clear, colorless, nonflammable liquid, having physical properties very similar to those of water. Rocket grade hydrogen peroxide (RGHP) is similar to HTP but with stricter impurity standards and is characterized in Military Specification MIL-P-16005 "Propellant Hydrogen Peroxide." For a summary of basic chemical properties, see Appendix A[19].

Hydrogen Peroxide (H_2O_2) as a propellant has a well established history. It was first discovered by Thenard in 1818[20]. Beginning with Helmuth Walker in 1938, hydrogen peroxide was seen as the mainstay of all rocket propellants. The United States Navy used it in 1955 in their Mk 16 torpedo and NASA used it for the X-15 and as attitude control thrusters for the Mercury spacecraft[21]. However, the advent of solid propellants and the development of the higher specific impulse hydrazine placed hydrogen peroxide on the backburner for several decades. Recently, however, interest in non-toxic and non-cryogenic propellants have brought peroxide back into the spotlight[22]. Russia still successfully uses hydrogen peroxide for their Soyuz vehicles[23]. Unlike hydrazine, the products of hydrogen peroxide are completely non-toxic. The pure liquid reaction of hydrogen peroxide is:

$$H_2O_2(l) \rightarrow H_2O(l) + ^1/_2\, O_2 = -98.2 \text{ kJ mol}^{-1} \qquad (1)$$
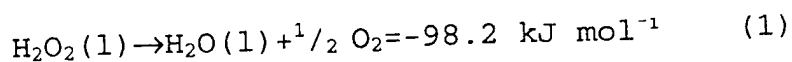
This exothermic reaction shows that complete decomposition yields superheated steam and oxygen as the products. All products are "green", and yield an expansion of 5233 times the liquid volume[24].

Not only is the per liter cost of HTP less expensive than hydrazine, the beneficial indirect effects will also make HTP a very viable and financially desirable option. Vapor toxicity adds costs to the development, qualification, and pre-launch handling, thus utilizing HTP will allow the total cost of thruster development to decrease significantly[25]. The United States Navy has initiated studies in order to introduce hydrogen peroxide powered onboard missile systems[26]. With safety a primary concern, peroxide has the potential to enable safe and reliable missile operations in the near future.

Other advantages HTP has are that it has a high density (87.5 lbm/ft^3 for 87%), it is storable as a liquid, it is non-reactive with the atmosphere, has a low vapor pressure, high specific heat, and it can use water as a referee fluid[27].

2.3 Safety and Handling of HTP

Hydrogen Peroxide, though considered non-toxic for the most part, does have a few safety considerations. Anyone working with it in any capacity should be well versed in the hazards and chemical characteristics of hydrogen peroxide.

HTP can cause mild to severe irritation to bodily tissue, depending on the concentration and the exposure time. If washed off and diluted with water quickly, skin contact has no long-term effects. Short-term contact will bleach the skin and will cause irritation without dilution.

The main danger is hydrogen peroxide contact with the eyes, which can cause ulceration of the cornea and permanent vision impairment if not treated promptly.

Prolonged inhalation can cause inflammation of the respiratory tract or nonspecific discomforts such as nausea, headaches, or weakness. These symptoms are reversible and usually disappear upon removal to fresh air.

Ingestion can cause irritation of the upper gastrointestinal tract and distention of the stomach and esophagus due to the rapid release of Oxygen. Gross overexposure by ingestion can be fatal[28].

In general, the effects are short-term and reversible as long as exposure is kept to a minimum and water is immediately applied to all spills and bodily contact[29]. As a minimum, safety glasses and gloves should be worn at all times when dealing with hydrogen peroxide. Reference Appendix B for a list of first aid measures dealing exclusively with hydrogen peroxide. See Figure 3 for the Hazard Symbol associated with Hydrogen Peroxide.
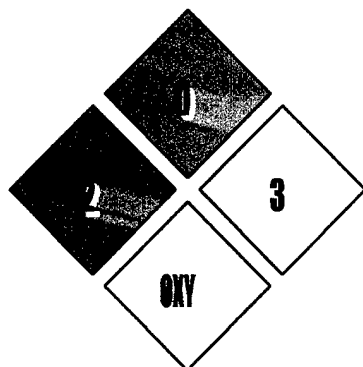
Figure 3. HTP Material Safety Data Sheet (MSDS) Hazard Symbol:
Red indicates fire hazard, blue indicates health hazard, yellow
indicates reactivity hazard and white indicates special hazards.

To use HTP as a monopropellant, a catalyst must be employed
in order to obtain rapid and efficient decomposition. Hydrogen
Peroxide can be catalyzed by a number of different materials,
proving both an advantage and a disadvantage. The advantage is
that the possible catalysts are so numerous that a cheap and
easily fabricated system is very feasible. The disadvantage is
that a speck of dust has been known to start an explosive
process[5]. Liquid spillage onto wood, paper, cotton, rags, or
clothing, especially those containing dirt or grease may
initiate combustion of these materials[30]. Therefore, great care
must be exercised to keep HTP isolated from any contaminants
such as metals, dust, and organic materials.

The largest concern of utilizing HTP as a propellant is
that even without a catalyst present, it auto-decomposes at
approximately 1% a year at room temperature[31]. For example, 1%
decomposition in a 20% ullage tank can raise the pressure by 250

psi[32]. This process can be slowed by storing in larger containers or by lowering the storage temperature. Chemical stabilizers can be added to protect against minor contamination, but tend to poison catalysts and dramatically reduce the decomposition efficiency. In either case, any long-term storage must contain a venting device such as a vent port or a relief valve to prevent pressure build-up and rupture of the container. For nanosatellite missions with short life times of 1-2 years, it may be feasible to design a HTP propulsion system that would not require venting.

The auto-decomposition of HTP also forces the storage environment to meet several specifications. HTP must be stored out of direct sunlight, away from combustibles and flammables, and close to a supply of water as well. Eyewash stations and safety showers in close proximity to operations are also necessary. Storage containers must be passivated to remove any unsuitable materials or extremely rapid decomposition and detonation could take place. A list of suitable and unsuitable materials is contained in the charts in Appendix C[33].

As mentioned previously, the rate of auto-decomposition is a function of the temperature. The decomposition approximately doubles for each temperature rise of 15° F. Table 1 shows the effect of temperature on decomposition.

Temperature (°F)	Approximate Decomposition Rate (@1 atm)
85	1%/year
150	1%/week
212	2%/day
285	Rapid with boiling (explosion if confined)

Table 1: Effect of Temperature on Decomposition of HTP[31]

While the acceptable range of temperature storage is between 12 and 105 degrees Fahrenheit[34], the logical conclusion is that it is safer to keep HTP cold or even frozen. An advantageous characteristic is that HTP contracts rather than expands upon freezing as water does. This property could allow HTP to be frozen during long duration missions without fear of rupturing hardware or plumbing.

After reading the safety considerations and potential hazards, some might question this propellant as being labeled as non-toxic. Overall though, if peroxide is handled with some common sense considerations, it is very easy to work with and is orders of magnitude safer than the traditional monopropellant choice of hydrazine. For example, hydrazine is a suspected human carcinogen and is lethal to fetuses, while peroxide presents no danger as a carcinogen nor has any reproductive effects. The result is that the ACGIH and OSHA exposure limits are two and one order of magnitudes lower respectively for hydrazine[35].

2.4 Procurement Issues

Unfortunately, high purity HTP is not easily procured. While hydrogen peroxide can be found in most medicine cabinets, this domestic quantity is usually under 3% concentration and packed with stabilizers. Few companies produce anything over 35% concentration, which is the commercial standard concentration used in the paper and textile industry. In commercial industry, only Solvay Interox (85%), Degussa-Huls (89.5%), and FMC (70%) produce high concentration HTP[36], though these concentrations are only available in large quantities (150kg drums).

There are several patents describing the process to distill hydrogen peroxide into higher concentrations (US#5670028, #5456898, #5232680,etc), but the process gets very expensive at higher concentrations, as the decomposition process is self-accelerating. For example, at 30% concentration, approximately one fourth of the peroxide molecules are lost as vapor as the peroxide bath is heated. This loss increases with the concentration. It has been found that the practical limit of concentrating by boiling off water is 85%. This research used a process developed at the Lawrence Livermore Laboratory to concentrate it higher under precisely controlled conditions[25]. This method should not be done without significant knowledge of the dangers associated with such a task. It is important to

avoid the detonation limit by keeping low temperatures and pressures.

Another significant issue with HTP is the transport of hydrogen peroxide. While the worldwide production capacity was 4.9 billion pounds/year in 1999[2], only 1.2 million pounds/year (0.02%)[37] were produced inside the United States. The lack of demand over the preceding three decades forced several U.S. companies out of business. As the demand is beginning to grow, several companies, such as Degussa-Huls are beginning to expand hydrogen peroxide production back into the United States. Currently, however, less than truck drum size quantities (~500 pounds) are very difficult to obtain. Due to auto-decomposition, aircraft are forbidden to carry high concentrations and the International Maritime Dangerous Code restricts drum size to less than 140 kg[38]. Federal Regulation 49CFR parts 100-185 cover the transportation regulations for concentrations up to 70% and parts 171-190 cover the vessel construction[27]. MIL-P-16005, Rev E are the specifications put together by decades of experienced peroxide vendors, with specifications above that of governmental regulations.

Section 4.5 describes in detail how 85% hydrogen peroxide was obtained and concentrated for this research.

2.5 Structure Compatibility Issues

Once HTP was chosen, the material to be used as the MEMS substrate was analyzed. While silicon was the primary candidate, it was initially unclear whether this was the best choice, given the reactivity of HTP and the stresses associated with a propulsion system.

Other materials that have been considered for substrate use are aluminum, diamond, and silicon nitride. Aluminum is the standard structure on larger satellites. Silicon, however, compares very favorably with aluminum in thermal conductivity, radiation shielding ability, and mass density. It is also seven times stronger than steel (in terms of maximum stress) and is transparent to IR radiation in the range of 1.2-6.5μm and 25-100μm wavelengths. Diamond is better in most all of the aforementioned areas, though the supply is much harder to get, thus contradicting the aim of cost savings and ease of fabrication. Silicon nitride has been presented as a possible alternative due to its extensive chemical inertness[5]. However, a lack of data on its use puts it beyond the goals of this project. The key factor is that the infrastructure to etch silicon is in place and is well established.

Silicon is listed as a Class 2 substance with HTP, meaning short term contact is acceptable. In a thruster design, contact will be minimized as it occurs only during thruster firing

operations and not during storage. The NASA-GSFC detector systems branch uses lower concentration peroxide to clean their silicon wafers and have not experienced problems with corrosion.

Because it was desirable to view the thruster before and during firings, a transparent cover was sought to be placed on one side of the thruster. Pyrex 7740 was chosen, as it is compatible with HTP. Also, Pyrex has nearly the same thermal expansion as silicon, thus reducing stresses during temperature changes[39]. This also helped the handling characteristics. Silicon is a very thin and brittle material and shatters very easily. Pyrex has a much higher strength and added support to greatly increase the handling ability of a single thruster.

Next, the melting points of all involved materials were considered. The expected flame temperature of 90% HTP is 1033.15K. The melting point of silicon is 1700K and is much higher for varying forms of Pyrex. Silver, the catalyst whose selection is defined later in Section 3.2, has a melting point of 1234K. Therefore, all major chemical and thermal compatibility issues with the substrate were satisfactorily addressed.

3. Prototype Thruster Design

3.1 Design Goals

The goal of this research was to design a working HTP catalytic MEMS thruster. A design methodology was developed so that the catalyst could be incorporated onto the MEMS device itself. Determining the length of catalyst needed to fully decompose the HTP was the major goal of the design effort. A catalyst section that is too long serves only to provide excessive volume to the system and one that is too short will allow liquid to get through causing a severe decrease in the propellant energy output. Several catalyst lengths were used to develop a model of ideal catalyst length and the results were used to determine if a catalytic MEMS thruster is a feasible option or if the required catalyst length exceeds the desired MEMS thruster sizes. During the design phase, the method of etching was undetermined. Therefore, the prototype thruster was designed conservatively to cooperate with a multitude of etch techniques. The result is a very linear design, with features larger than the capabilities of some etch techniques. The following sections will cover the issues and the design of the major thruster elements.

3.2 Orientation

Two main orientations in which a MEMS thruster can be constructed were considered. The first, which is modeled after DARPA's digital microthruster[10] and JPL's subliming solid microthruster[7] is a stacked design. In this approach, several layers of wafers are stacked to form the thruster. The catalyst would consist of a nano-scale mesh made of or sputtered with a catalyst material. This design option can be seen in Figure 4.
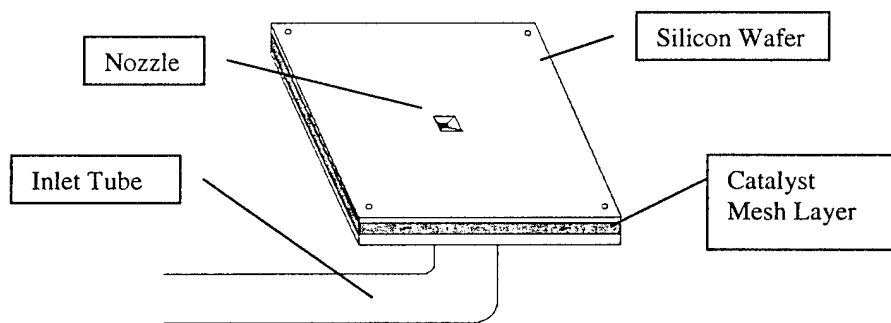
Figure 4. MEMS Thruster Stacked Approach

The second orientation is one modeled after MIT's design for nozzle work[8,11], which places the propulsion system on a single wafer. This design is shown in Figure 5. This method is limited in the aspect of the nozzle and therefore has a decreased efficiency. However, the advantage is that the catalyst surface area can be increased relatively easier in this design by simply elongating the catalyst section. In the

previous approach, several layers of mesh would have to be
constructed and adhered to get similar surface areas. Because
one of the goals of the research effort was to study the effect
of varying catalyst lengths, the axial layout approach was
chosen.
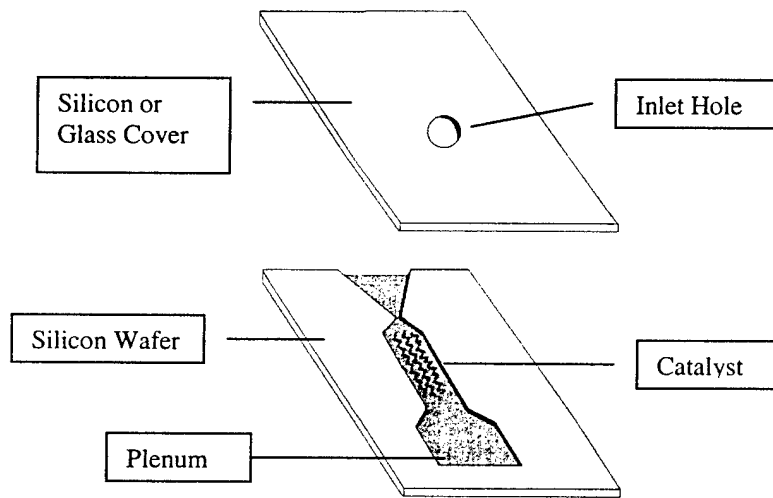
Figure 5. MEMS Thruster Axial Approach

3.3 Catalyst

3.3.1 Catalysis Kinetics

Developing a catalyst that would efficiently decompose
hydrogen peroxide and could be incorporated on a nano-size
thruster was the most significant design consideration of this
research effort.

Before considering the specific design, it is important to
understand the role of a catalyst in a thruster. HTP auto-
decomposes, but at a very slow rate. Catalysis provides an

alternate path of lower activation energy by which the reactants

can become products. In a reaction, the reactants form a

transition state, a symbolic state that the reactants must pass

through in order to form products. A catalyst lowers the energy

of this transition state significantly, while the energies of

the products and the reactants remain unchanged. Figure 6 below

exemplifies this process.
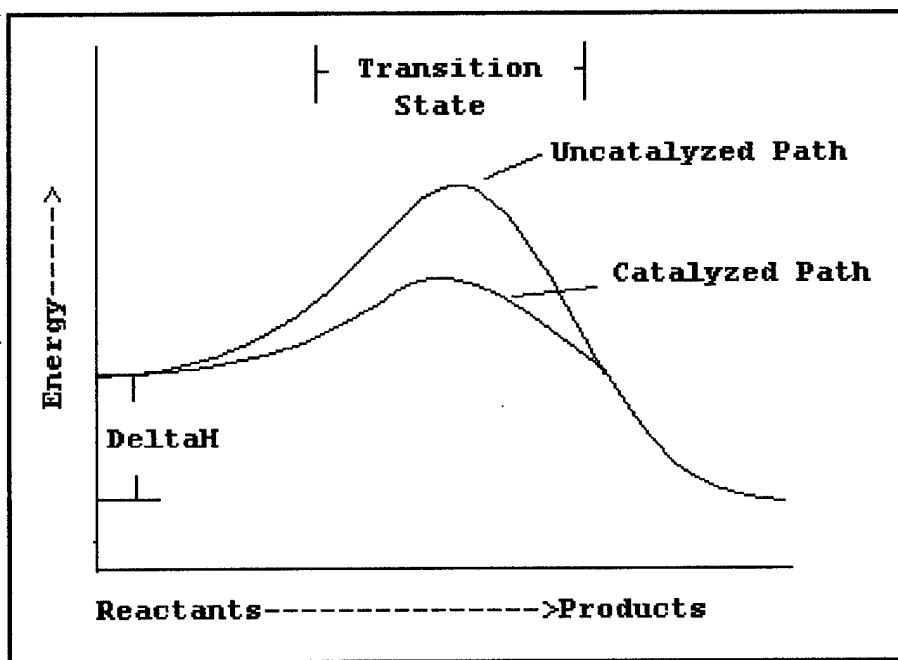
Figure 6. Catalysis Kinetics. Delta H is the
difference in energy of the products and the reactants.[40]

Since the lower energy path is the one of least resistance,

a higher proportion of the total molecules will have the energy

necessary to react than they would have on the uncatalyzed path.

Therefore, the rate of the reaction is greatly increased. It is important to note that there is no change in free energy in this reaction as the energy of the reactants and products remain the same. The decrease in activation energy applies to both the forward and reverse reactions; therefore the chemical equilibrium will not change. This means that the steady state reaction is unchanged. A catalyst simply speeds up the processes.[40]

Heterogeneous catalysis operates when a reaction is catalyzed on a surface. The reacting species are 'attached' through adsorption at active sites, places where the catalyst is present. These active sites serve as a changing station, where the HTP can decompose in the presence of a catalyst. An optimum design would therefore maximize the available active sites.

3.3.2 Options

There are several proven catalysts for HTP. Platinum, iridium, silver, palladium, and ruthenium have all been tested and have successfully reduced HTP[41]. Silver has proven to be one of the more easily attainable and reactive transition metals, and for this reason, it was chosen as the catalyst material for this work. Several methods of employing silver in a catalyst bed have been used. Silver electro-plated stainless steel screens have been used, but they have large pressure drops and

are easily poisoned[15]. Another potential problem is the flame
temperature of very high concentrations (>90%) of HTP exceeding
the melting point of silver. Silver-plated nickel has been used
to increase temperature capability for >90% concentrations, and
silver wire cloth was also used at Lawrence-Livermore
Laboratories[25]. The problem was avoided in this project by
maintaining hydrogen peroxide concentration levels between 80%
and 90%.

Each catalyst has a widely varying reactivity however. A
study at Purdue showed a comparison of reactivity of HTP with
several catalysts and their corresponding oxides[21]. Their data
shows low reactivities for lead oxide, with the highest
reactivities going for ruthenium oxide. Most importantly, the
study showed a low reactivity of silver oxide (AgO) as compared
to bare silver, which has a high reactivity. Therefore, the
prevention of oxide formations appears necessary. This supports
earlier findings of "increasing performance" catalyst packs,
that could result from the peroxide slowly stripping off the
oxide layer and getting to the higher reactivity bare silver[42].

3.3.3 Surface Area

Also of major concern is the available surface area (and
therefore active sites) the catalyst has for the propellant to
contact. Several innovative approaches have been used to

maximize surface area. Beds of pellet-type structures, honeycomb cordierite containing multiple cells, and catalyst meshes are a few examples. However, most of these processes cannot be reproduced on the MEMS level. Silver, for example, tends to become planar as the size decreases[43], thus effective pellets cannot be easily formed. Technology does not yet exist to create cell-containing ceramic supports at these length scales. These limitations forced a new type of catalyst design.

The types of features that can be created on a silicon wafer are very limited. Variable-geometry channels are one of the primary features available. The ability to place an independent catalyst into this channel is very challenging. Therefore, the channels were utilized as the catalyst themselves. This was done by etching small channels immediately preceding the nozzle throat. These channels were then vapor-deposited with silver. Effectively, the thruster has small channels made of silver for the peroxide to flow through and decompose. Several catalyst geometries were analyzed in a fixed width, fixed length bed. The goal was to maximize surface area given the etch ability (~20 microns as the smallest feature). Figure 7 shows the different designs used. Only straight sided features were designed in order to accommodate the many different etch techniques. The designs consisted of a single zigzagging channel, three straight channels, three zigzagging

channels, and several block pillars. Figure 8 then shows the
effective surface area available for catalysis for each design.
Calculations can be found in Appendix D.
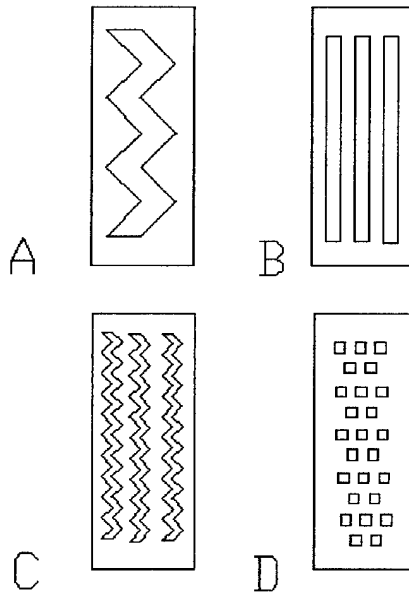
Figure 7. Possible MEMS Catalyst Geometry Designs
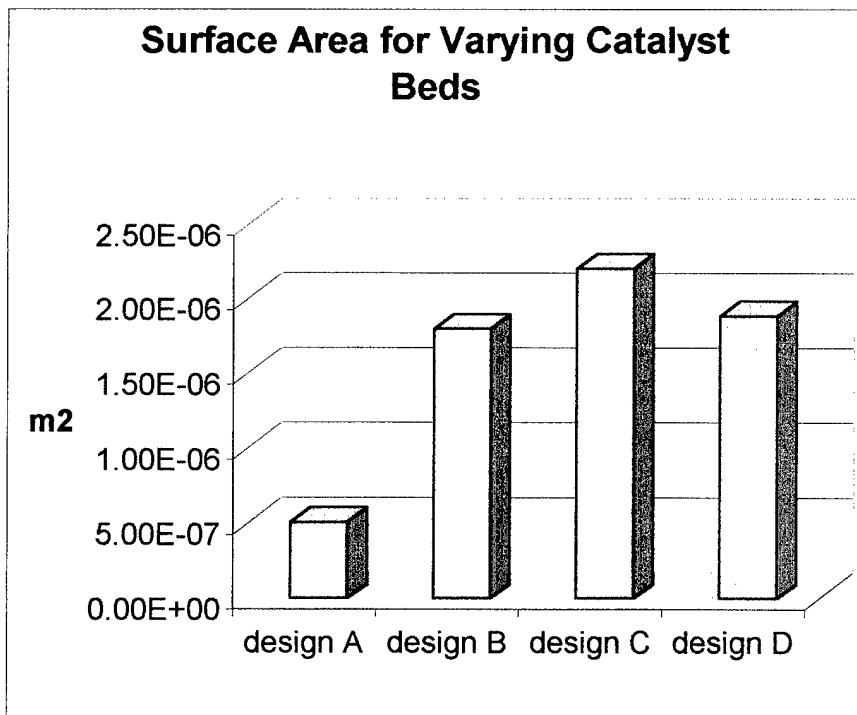
Figure 8. Surface Areas for Varying Catalyst Designs

It is readily seen that multiple zigzagging channels appear to be the optimal design to maximize the available surface area.

3.3.4 Length

The key, and perhaps least understood parameter is the appropriate length of the catalyst. It is obviously desirable to have the catalyst as short as possible to minimize the overall size of the thruster. However, the HTP must fully decompose in the time it spends in the catalyst. This introduces the idea of residence time, which can be thought of as a time of occupancy. The residence time is thus a function of the velocity of the fluid and the length of the catalyst. If a critical residence time, a length of time required for full decomposition of HTP, was known, the proper critical length catalyst could easily be designed. However, this critical time changes with different catalyst materials and is also a function of temperature and pressure. The result is that the traditional approach of catalyst length design is to use empirical data of a length that has already been proven to work for a range of flow rates and pressures. As MEMS thruster technology is fairly new, no such data exists for miniature catalysts with minuscule flow rates and pressures. Therefore, several catalyst lengths were designed in this work and the percent decomposition was

determined for each. It then became possible to develop a model of critical times in the MEMS thruster.

To establish a baseline catalyst length, "rule of thumb" catalyst lengths widely accepted across the aerospace community for larger HTP thrusters were used and scaled down to the MEMS sizing of interest. While most fluid dynamics laws cannot be scaled linearly to this level, this was used only to get an order of magnitude estimate.

A generally accepted catalyst length for larger peroxide thrusters is 7.5cm(~3"). The United States Air Force Academy tested a catalyst at this exact length for an HTP engine with 0.4kg/sec of mass flow rate[44]. This catalyst proved successful, producing clear superheated steam, a sign of complete decomposition. Using these numbers, it is observed that a mole of HTP spent 0.53 seconds in contact with the catalyst bed. Using that time and a desired flow rate around 390 micrograms/sec (discussed in Section 5.2) for these MEMS thrusters, the effective catalyst length must be around 1.7mm (see Appendix E).

In another report, the decomposition rate is related to temperature and "in temperate conditions…full decomposition was reached after 0.025 to 0.05 seconds but at 0°C the starting delay was near 0.5 seconds."[42]

31

Apparently, the field of describing peroxide catalyst activity is one that has widely varying opinion and has yet to reach a point where it can be defined with great certainty. Using these baseline numbers though, five different catalyst lengths were designed. Three were under 1.7mm effective length and two were larger than 1.7mm effective length. Table 1 shows the effective and actual catalyst lengths for the thrusters.

Design:	Actual Length (μm)	Effective Length (μm)
1	2500	3535
2	1500	2121
3	1000	1414
4	750	1061
5	500	707

Table 2: Actual and Effective Catalyst Length Designs

3.4 Nozzle

Another key design parameter in a MEMS thruster is the nozzle. The use of extremely small dimensions causes the thruster to operate in a fluid dynamics regime somewhat unfamiliar to thruster design. While the study of the fluid dynamic behavior in this regime is beyond the scope of this particular paper, some of the work done in the field will be discussed and used to design the MEMS thruster.

For the thrust and flow rate levels of interest, the flow is characterized by very small Reynolds numbers, where Reynolds number can be defined by:

$$R_e = \frac{\rho U D_t}{\mu} \qquad (2)$$

where ρ is density, U is the fluid velocity, D_t is channel width and μ is the coefficient of viscosity.

As smaller features cause the Reynolds number to drop, the Knudsen number increases. The Knudsen number is defined as:

$$Kn = \frac{l}{H} \qquad (3)$$

where l is the mean free path of the gas and H is the characteristic device scale length.

With these high Knudsen numbers (>.01), the continuum assumption used to derive the Navier-Stokes equations may no longer be valid. For example, one condition violated is the "no-slip" boundary condition, which states that the fluid velocity at the wall in a structure is zero. Slip begins to occur at high Knudsen numbers and it has been suggested that the following condition can be inserted into the Navier-Stokes in place of no slip with a high degree of accuracy[45]:

$$u\big|_{y=0} = \frac{2-\sigma}{\sigma} Kn \frac{\partial u}{\partial y}\bigg|_{y=0} \qquad (4)$$

where u is the tangential velocity, Kn is the Knudsen number, y is the distance from the wall and σ is the coefficient of tangential momentum accommodation. As the Knudsen number continues to increase (smaller channels), this slip condition modification no longer provides accurate solutions and other methods must be employed. Numerical methods such as Direct Simulation Monte Carlo (DSMC) are one possibility. This is a very computationally intensive approach. Case studies have shown that velocity slip has little effect on the final performance of the nozzle and therefore was not considered[46].

The major issue considered in the MEMS nozzle was assuring that the boundary layers did not grow so large as to prevent choked (supersonic) flow. Rae[46] found that small divergence angles and low Reynolds numbers create large viscous boundary layers that can completely fill the nozzle and create a shockless transition to subsonic flow. This is caused by thermalization of the flow, which allows the kinetic energy to be transferred into thermal energy. However, it has been concluded that sonic flow can be achieved in these small nozzles with incorporation of greater than average divergence angles[46].

Kim[46] tested the tradeoff between viscous losses due to large boundary layers and the non-radial thrust losses caused by a highly divergent nozzle. His conclusion was that the viscous

losses dominated. For example, his "radially efficient" 20-degree nozzle was greatly outperformed by his 30-degree nozzle, which prevented the boundary layers from merging. Widely accepted nozzle design processes call for 15°-20° nozzle divergence angles for optimal performance. Using this data, MEMS thrusters for this project were designed with the theoretical optimal half angle of 17°, and with larger 28° half angles in order to validate Kim's data as well as to remove the viscous loss static from the experiment. The nozzle throat was set at 30 microns for both designs. This is slightly larger than the filter distance of 25 microns, which is close to the conservative lower limit of high-resolution etches. Expansion ratios of 10:1 and 16:1 were used in order to obtain high exit Mach numbers.

Experimental data has been collected by several sources[45,46] representing the efficiency of nozzles as the chamber pressure drops (which causes decreasing Reynolds numbers). Rae and Kim's paper documents sufficient data to show that the specific impulse (ISP) efficiency begins to drop dramatically at low Reynolds numbers and also that the inviscid and viscous solutions (for mass flow rates) are similar. For design purposes, these results were used to predict a 20% degradation in theoretical performance. This was subsumed in the ISP efficiency term in the expected results (reference Section 5.2).

3.5 Injector

An injector is desired in a MEMS thruster for the same reasons they are used in larger thrusters. An injector provides a pressure drop, which imparts injection velocity to the flow. Additionally, the differential pressure keeps any combustion disturbances isolated from the propellant feed system.

Designing for a baseline 20% pressure drop[47] across the injector, the injector area is given by:

$$A_{inj} = \dot{m} \sqrt{\frac{2.238K}{\rho \Delta P}} \qquad\qquad (5)^{[47]}$$

where $\dot{m}$ is the mass flow rate, K is the head loss coefficient, ρ is the density and ΔP is the pressure drop. K will be defined as 1.5 for a sharp edge orifice.

The results show that for a chamber pressure of 5 psi, the area of the injector necessary is approximately $1.09 \times 10^{-10} m^2$. With a nominal etch depth of 300 μm, the width of the injector would be 0.36 μm. The smallest feature that can be designed, without knowledge of the etching technique that can be acquired, is around 20 μm. Because the desired injector size was significantly beyond the etch capabilities for this design, an injector was not included. The effect of not including an injector is investigated in Section 6.4.1.

3.6 Valve

As this is a liquid fueled system, a valve must be integrated to control the flow of propellant. However, there are no flight qualified MEMS microvalves at the time of this research[48]. The Aerospace Corporation has experimented with limited stroke silicon valves, but they introduce great flow impedance[45]. A suitable MEMS valve needs to be developed, but that work is beyond the scope of this effort, therefore this thruster was designed without a MEMS valve. For test purposes, a small Commercial Off-The-Shelf (COTS) valve was connected just after the propellant tank, prior to the connection with the MEMS thruster. However, future applications of this thruster will require a study into the feasibility of valves at this level. Current plans at NASA GSFC include having Marotta Scientific Controls build upon their work on cold-gas MEMS valves in order to produce a HTP microvalve for this thruster. Their primary goal will be to build a MEMS valve capable of providing the specifications required. For this effort, it was sufficient to define the valve specifications needed for a MEMS thruster. Expected operating conditions were compiled and restrictions desired for making this feasible for use on a nanosatellite were applied and listed. Valve cycle times were determined from the desired impulse bits for nanosatellites and stringent leakage

constraints were applied due to the small propellant volume

expected. Table 3 is a summary of the specifications that are

required for a MEMS thruster valve.

Operating Voltage:	< 5V
Response Time:	0.1 second with a 1.0 second duty cycle
Working Fluid:	~90% Hydrogen Peroxide
	No trapped liquid
*Note	Trapped H_2O_2 will naturally decompose and cause extreme pressure build-up w/o venting
Internal Leakage:	< 1×10^{-5} sccs (Gaseous Helium)
External Leakage:	< 1×10^{-5} sccs (Gaseous Helium)
Inlet pressure:	25 psia maximum
Max differential pressure:	25 psid
Pressure Drop:	0.1 psi
Flow Rate:	200-700 ug/s at approximately 5 psia
Cycle Life:	10,000 cycles, open to close
Temperature Range:	10-40° C
*Note	A design goal of 0-50°C shall be maintained.

Table 3: Desired Micro-valve Specifications

The thermal constraints listed are standard for an orbiting

spacecraft, but it was important to determine whether this range

is still valid for small MEMS systems that will have high

temperature combustion taking place inside of a high thermal

conductivity material such as silicon. A simple thermal

model was set up as seen in Figure 9.
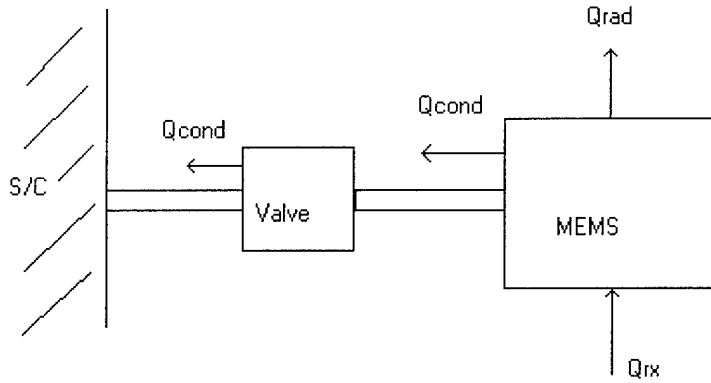
Figure 9. MEMS Valve Thermal Analysis. Q_{cond} is the conducted
heat, Q_{rad} is the radiated heat and Q_{rx} is the heat
of reaction.

Environmental effects were neglected. The maximum combustion

temperature served as the reaction heat, while radiative and

conductive effects were accounted for. Conduction was modeled

using the Fourier Law:

$$q = -KA\frac{\Delta T}{\Delta X} \tag{6}$$

where q is the heat transfer, K is the thermal conductivity, A

is the cross sectional area, ΔT is the temperature difference,

and ΔX is the distance between the hot and cold locations.

The Stefan-Boltzmann Law was used to model heat radiation:

$$q = \sigma \varepsilon A T^4 \tag{7}$$

where σ is the Stefan-Boltzmann constant, ε is the emmissivity of

the silicon, A is the black body area, and T is the temperature.

The analysis shows that the 50°C equilibrium temperature limit could be reached in the valve. However, assuming the connection bridge was made of silicon, there would have to be at least 67 cm of separation between the valve and MEMS thruster. This is obviously impractical for a nanosatellite, as the overall expected diameter would be much smaller than this. The high thermal conductivity of silicon is the dominating factor. This is obviously not feasible for incorporating the thruster and valve on the same chip with this separation distance. This leads to the conclusion that there must be some thermal isolation or active thermal dissipation designed into a flight system. Replacing the bridge with a lower thermal conductivity material would significantly reduce the needed displacement and may be the best solution.

3.7 Plenum

A plenum is designed as a receptacle for the propellant prior to entering the catalyst. The plenum was designed slightly larger than 1mm in order to accommodate inlet from a 1mm diameter propellant line.

At the aft end of the plenum, a set of stacked pillars are implemented as filters. The spacing between the filters is 25 μm, the smallest distance that can be comfortably designed to accommodate wet or dry etching techniques. The filters perform

the function of removing any large particles that may obstruct

the catalyst or the nozzle. These particles may be present in

the propellant, or they may be inherent in the thruster itself

after excessive handling from bonding, dicing, and integrating.

The filter also serves as a pseudo-injector, possibly limiting

backflow.

Immediately after the filters, the plenum will transition

to the smaller catalyst section. It is necessary that this

transition be smooth to limit boundary layers and flow vortices

from forming.

3.8 Final MEMS Design

All of the considerations discussed in the previous

sections were combined to create final thruster layouts. Each

thruster consists of a nozzle, a catalyst bed, and a plenum with

a built-in filter to initially be etched 300μm in a 500μm wafer.

Figure 10 shows a sample thruster design.
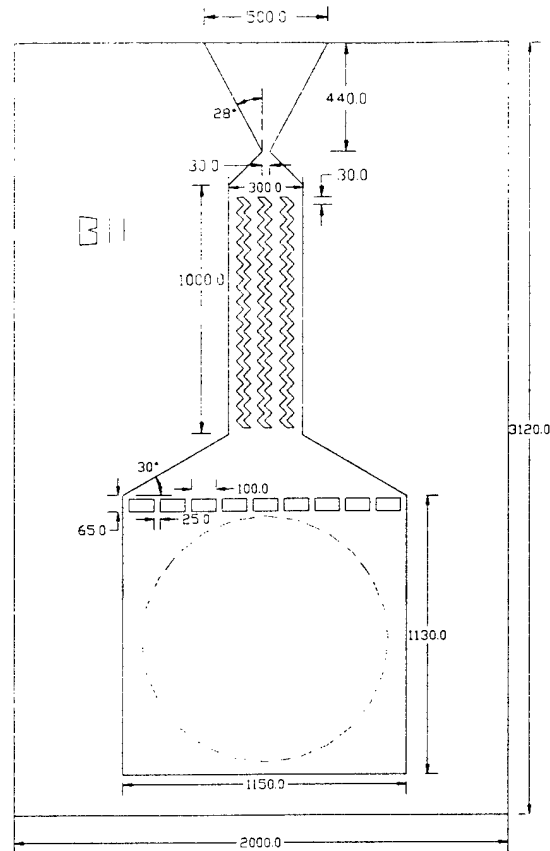
Figure 10: Sample Thruster Design. All units are in microns.

Two different inlet designs were also incorporated. The lateral integration design requires an inlet hole in the glass and has a confined plenum area. This is the design seen in Figure 10. The longitudinal design does not require any special features to be etched into the glass. This design is merely an extended plenum, which reaches to the edge of the silicon. Integration is performed by flowing propellant through the thruster from the side. While the latter method has a more imperfect sealing scheme, it was designed in case problems arose

with the glass etching. It was also desired to have pressure

taps on a few of the thrusters in order to validate the chamber

pressure.

In order to test all of these different parameters (exit

area, catalyst length, and integration scheme), a total of

seventeen designs were created. Between eighteen and twenty

thrusters of each design were then laid out onto a single wafer

to account for problems during etching or fractures during

handling. Each design was identified with an ID number, which

was etched into the chip. The designs were then integrated

together into a mask. The final result is a 100mm diameter

wafer mask that contains the blueprint for 324 thrusters. This

layout can be found in Appendix F. Table 4 describes the

variation in the thruster designs as associated with the ID

numbers.

Design ID #:	Nozzle Exit Width (μm):	Catalyst Length (μm):	Pressure Tap:	Inlet Design:
1	300	1000	N	LATERAL
2	300	1000	N	LONGITUDINAL
3	300	750	N	LATERAL
4	300	750	N	LONGITUDINAL
7	300	500	N	LATERAL
8	300	500	N	LONGITUDINAL
9	500	1000	N	LATERAL
10	500	1000	N	LONGITUDINAL
11	500	750	N	LATERAL
12	500	750	N	LONGITUDINAL
13	500	750	Y	LATERAL
14	500	750	Y	LONGITUDINAL
15	500	500	N	LATERAL
16	500	500	N	LONGITUDINAL
17	500	1500	N	LATERAL
18	500	1500	N	LONGITUDINAL
19	500	2500	N	LATERAL

Table 4: Design Variations for the MEMS Prototype Thruster

Figure 11 shows the basic design of each thruster.
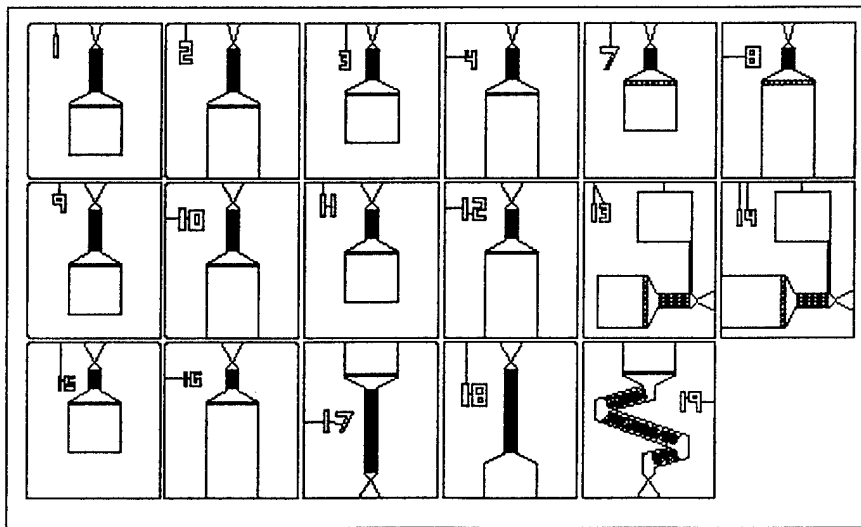
Figure 11. Prototype MEMS Design Variations

Noticeably missing are design iterations 5 and 6. These designs were eliminated due to lack of room on the wafer and to simplify the layout. Thruster #19 contains a multi-faceted catalyst channel in order to maximize effective length and to circulate propellant flow onto the catalyst walls. Notches were designed into the corner of each thruster so that when combined, a crosshair would be created for eventual dicing. All designs were arranged and drawn in AutoCad 14™. They were then converted into AutoCad 12™ format in order to be imported as GDS II files. These were the necessary file formats for photoresist creation.

4.CONSTRUCTION

4.1 Etching Process and Results

The fabrication process is based on deep reactive ion etching (DRIE) of 100 mm diameter, 500 μm thick silicon wafers. The DRIE, manufactured by Surface Technology Systems (STS), has the capability of anisotropic through-the-wafer etching with vertical sidewalls of a pattern defined by an etch mask on the front surface of the wafer. The use of photoresist as the masking material allows the etch mask to be defined by a simple photolithographic process with dimensional tolerances of several microns.

The fabrication begins by applying a six-micron thick layer of photoresist using a spinning process. After a soft bake to drive off excess solvents, the photoresist is exposed to ultraviolet (UV) light through the photomask. The photomask is a glass plate with metal patterned in the design desired for the application. In this case the patterns are the various designs of the thruster with the nozzle, catalyst fins, filters, and plenum. The opaque areas of the photomask prevent the UV from exposing the photoresist where it is to remain as the etch mask. The photoresist is then developed to remove the areas exposed to the UV and hard baked to remove residual developer solvents, promote adhesion, and harden the photoresist[49].

The wafer is next placed in the DRIE system and the area not coated with photoresist is etched. An etchant gas flow (SF_6) and a passivation step are alternated. After a specified etch time, C_4F_8 is used to coat the exposed areas and passivate the surface[46]. Once etchant flow is restarted, the exposed areas normal to the flow are cleared of the coating, while still protecting the walls from indirect etchant exposure. The etching is stopped when the desired depth is reached. The wafer is removed from the DRIE and the photoresist is removed with solvents.

This project became one of the first tested on the new STS DRIE at NASA Goddard Space Flight Center. The first wafer that was etched showed relatively good detail with a few problem areas. First, the trenches were not completely vertical. The etch resembled a wet etch, where the material removal was evident in the horizontal direction. Therefore, the walls were curved and over-etched. Sharp features such as the throat were also rounded. The main problem was etching the filters. The tall and slim filters could not withstand the uneven etching and in every thruster, the center 5 or 6 filters collapsed. Figure 12(a) depicts this. An interesting observation was that the two filters closest to each side managed to stand in nearly every thruster.

The center features are small compared to the large void of the plenum and horizontal etching was magnified. The filters closest to the wall are 'protected' by the walls and other features, and therefore still stand.
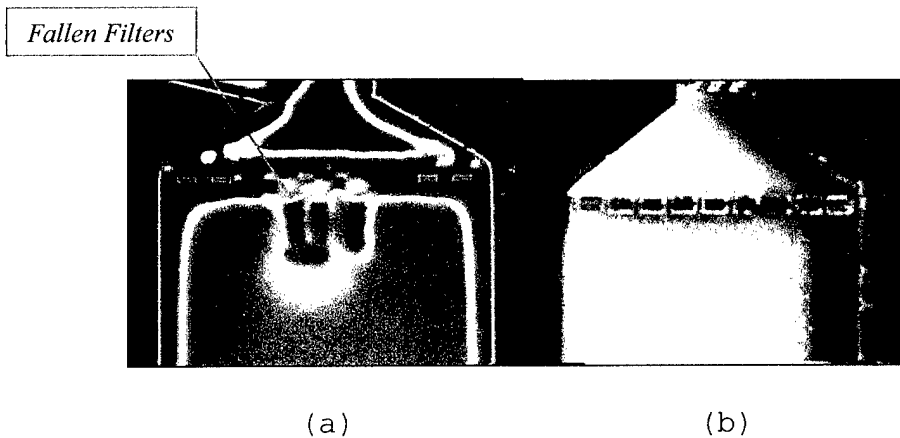
Figure 12. MEMS Filter Results from First and Second Etches
    a) Wafer with collapsed filters (First Etch)
    b) Wafer etched to specifications (Second Etch)

The next several wafer etches dramatically improved as the appropriate program was run on the DRIE for the etch type desired. Finally, a wafer nearly identical to the drawing in every way was produced. All filters stood and all features were sharp with very straight walls as seen in Figure 12(b).

4.2 Deposition

An aluminum shadow mask was created using the same techniques used to create the photomask. The shadow mask's purpose was to allow silver to be evaporated onto the catalyst fins. To deposit the silver catalyst, the etched wafer was

placed in a holder and the shadow mask was taped to the wafer
and covered the entire thruster except for the catalyst region.
The holder, wafer, and shadow mask were placed in a vacuum
deposition chamber held at a base pressure of at 1×10^{-6} torr. A
Denton e-beam evaporator then deposited 99.999% silver onto the
catalyst region at a rate of 5 angstroms/sec. The procedure was
stopped after 32 minutes of deposition for a total silver
coating of 1μm. Figure 13 shows a wafer after silver
deposition.
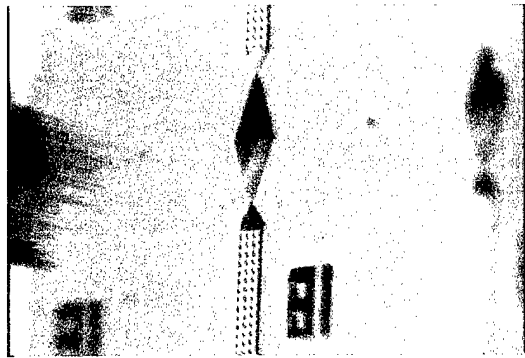
Figure 13. MEMS Catalyst after 1μm Silver Deposition

4.3 Bonding

A glass plate was then anodically bonded to the silicon
wafer. This closed off the system and allowed a convenient
viewport. For anodic bonding, a sheet of pre-ultrasonically
drilled Pyrex was placed over the etched side of the wafer to
seal the thrusters. The silicon-Pyrex stack was then placed on
a hot plate and heated to 300-400° C. A negative voltage of 700-
1200 V was applied to the Pyrex via a pinpoint contact while the

silicon was kept at ground potential. Bonding can be completed within several minutes for substrates connected with smooth surfaces[49]. These surfaces, containing many channels and chambers, took about half an hour to complete. Bonding could be observed as a constantly expanding dark ripple forming from the voltage contact. During this process, the silver appeared to bronze and darken. This was due to oxidation of the silver by the application of heat and voltage in ambient conditions. As expected and validated in Section 6.6, this had a detrimental effect on the catalyst and prevention of this oxidation process was necessary. Therefore, a method to purge the oxygen from the immediate vicinity of the wafers was sought. A vacuum glove box for hazardous chemical operations was modified for this application. The hot plate and voltage source were placed inside the glove box while argon was used to purge the interior of the box. The bonding process was completed in this environment. No oxidation was observed during this process.

The completed silicon-Pyrex wafer was then diced by diamond saw into the individual thrusters at the crosshairs. It was discovered that the saw blade was larger than expected and after one cut, the crosshairs were cut away entirely. Therefore, visual estimation had to be employed once the wafer was rotated for cutting in the other direction.
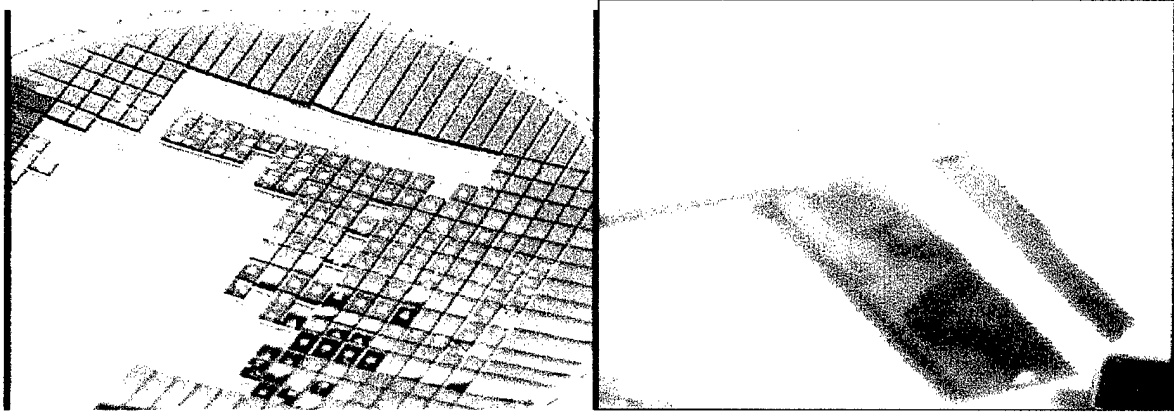
Figure 14. Diced Wafer (left) and Individual Thruster (right)

This did not present a problem as the exact cut was done on the dimensionally critical side of the thruster (nozzle/inlet) and the visually-guided cutting took place only on the side cuts.

After dicing, the wafer was kept in water and the individual thrusters were removed underwater and then flushed with running water to prevent the saw lubricant from filling the channels and drying. Figure 14 shows the thrusters just after dicing and Figure 15 shows a comparison of the completed thrusters to a penny and a human hair.

Human Hair
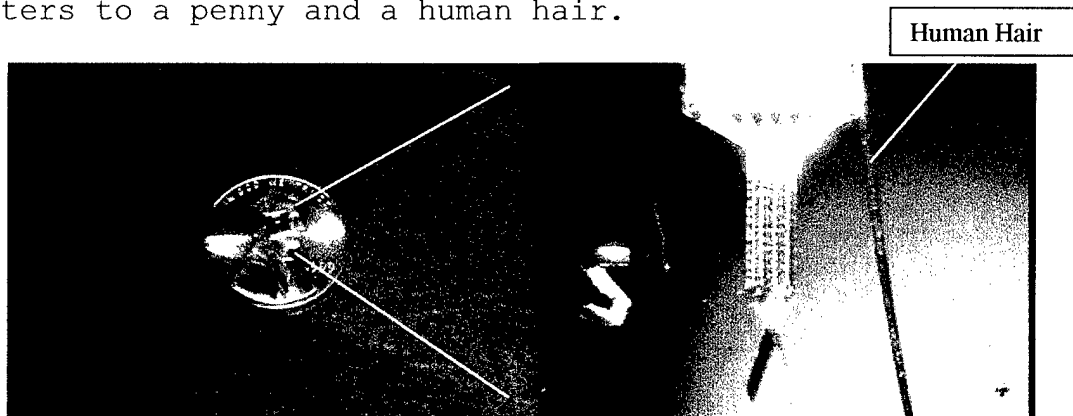
Figure 15. Completed Thruster Size Comparisons

4.4 Packaging

One of the more challenging parts of developing a MEMS system is integrating it with the macroscopic world. This issue includes packaging, as well as integration with any desired electrical connections.

There are two different integration schemes for the thruster, corresponding to the two major design subsets described earlier. The preferred design is the lateral integration as can be seen in Figure 16(a). In this method, the glass is counter bored (1mm diameter and 0.5mm diameter) and a 1mm feed tube is epoxied into place. While it is easy to attach the feed tube in this method, having very thin glass cut, polished, and ultrasonically drilled represents an expensive investment of time and money. The drilled glass could not be procured in time for this effort, however longitudinal integration was accomplished as indicated in Figure 16(b).

(a)   (b)
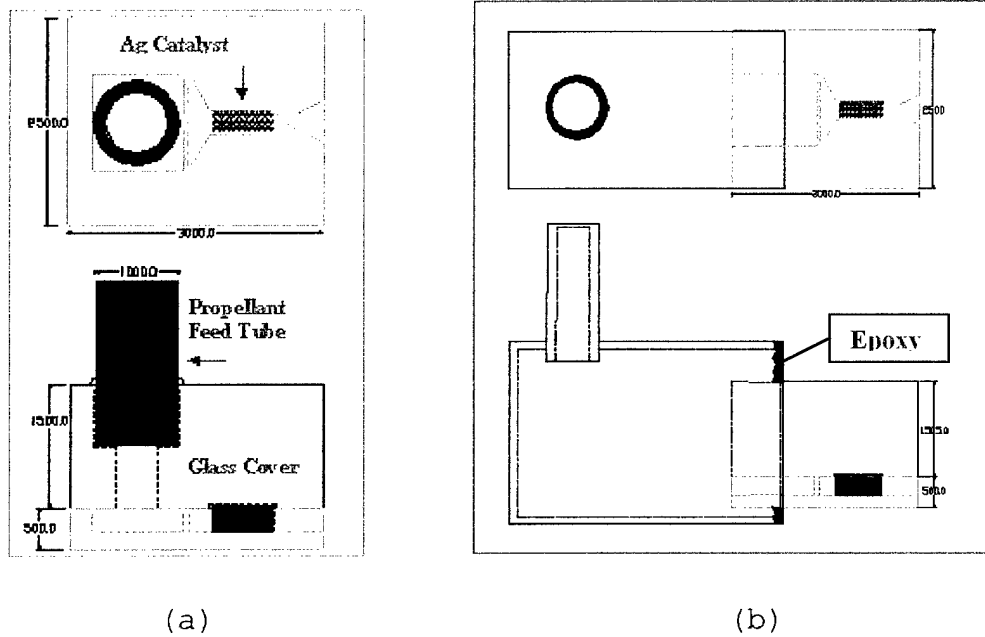
Figure 16. Macro-Integration to Feed Lines (units are in microns)
(a) Lateral Integration Scheme
(b) Longitudinal Integration Scheme

The advantage of longitudinal integration is that no holes are required in the glass. A 0.075″ piece of flat glass was obtained and bonded. Only the longitudinally designed thrusters were removed on the first run. For this method, a 2.5mm tube was cut to have small slits in the opening to hold the thruster into place. The top and bottom openings were then epoxied shut. This can be seen in Figure 16b.

The open end of the tube from either integration scheme was then be connected to a syringe needle for flow testing (Figure 17 bottom) and to a tank for actual firings (Figure 17 top). The syringe was placed in a Genie™ syringe pump, which can apply

a constant load (and constant pressure) at very small flow rates
to remove any instabilities with a pressure fed system.
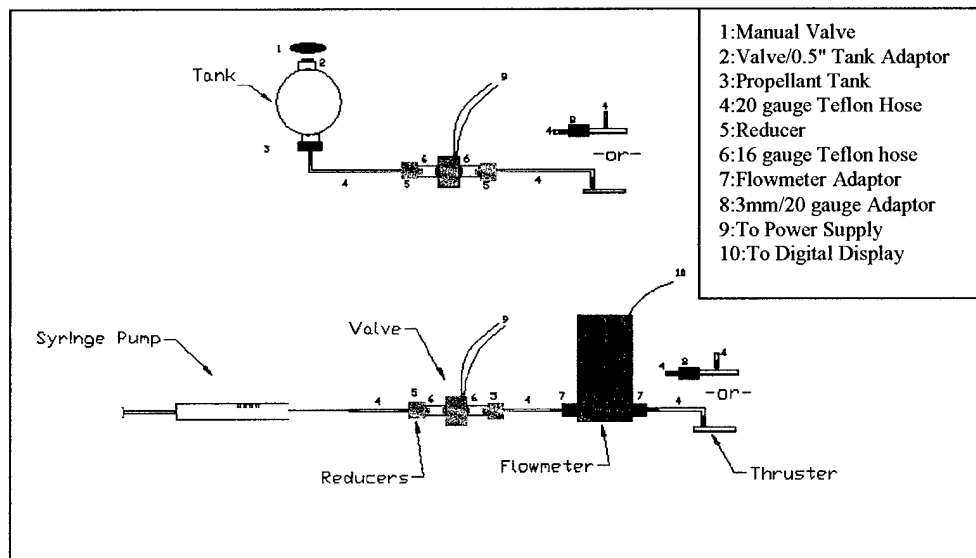
Figure 17. Propellant Feed System Layout for Thrust
Tests(top) and Decomposition Tests(bottom)

4.5 HTP Production

As widely documented, obtaining high concentration HTP is a
daunting task. After running into dead ends through most U.S.
sources, Degussa-Huls sent two 500mL samples of 70% Hydrogen
Peroxide for use in this work. One sample was high purity grade
(electronics grade) containing little of the stabilizers
typically present. 35% Hydrogen Peroxide was purchased from
Fischer Scientific to test concentration over large
differentials as well.

To concentrate peroxide required a lab set up similar to
that documented by Whitehead[25]. A Yamato RE500 Rotary

Evaporator, a water heater, a dual water aspirator, and a chiller were purchased and integrated. Figure 18 shows the setup in the NASA GSFC Advanced Chemistry Laboratory. The rotary evaporator takes advantage of the fact that water and hydrogen peroxide have two different boiling points (100°C and 150°C respectively). Since water and hydrogen peroxide do not form an azeotrope, distillation is a viable option for separation[50].

The distillation process used was as follows:

First, the chiller (Figure 18 far left) was turned on to 4°C and circulation was started. Then, the aspirator (middle) was turned on and the vacuum was observed through a gauge between the aspirator and evaporator. The water heater (bottom right) was heated to 80°C while between 10 ml and 100 ml of 70% HTP was loaded into the evaporation flask. The rotary evaporator (right) was then turned on to 20 rpm and then the flask was lowered into the water. The rotation allows a thin film of peroxide solution to form, from which the water can easily evaporate. The water condenses on the cold condenser coils and gathers to drip into a collection flask. The aspirator was used to pull a vacuum on the entire system, thus avoiding the detonation limit for peroxide and allowing safe operation. The

overall result is that the water is selectively evaporated out of the system.
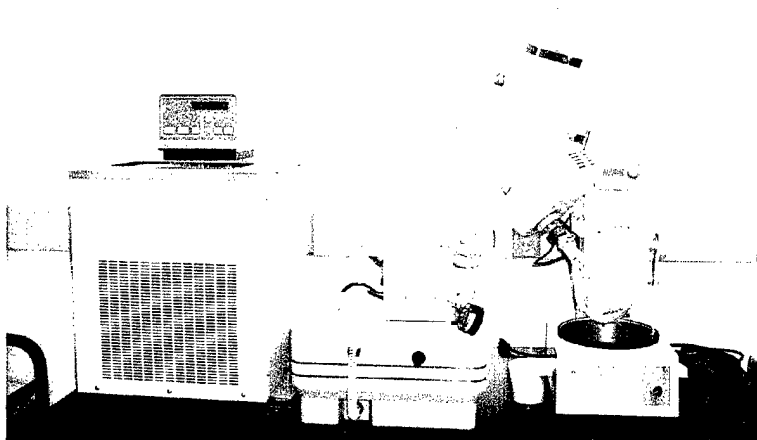
Figure 18. HTP Distillation Set-up: From left to right is the chiller, aspirator, and rotary evaporator.

It was discovered that the key to successful distillation was the vacuum level obtained. During the first two tests, the maximum vacuum capability of the system was 25mm Hg (measured below ambient). Very little change of concentration was observed over long periods of time (>2 hours). A T-junction was then acquired and inserted to take advantage of both vacuum ports on the aspirator. The maximum vacuum obtained was now 28mm Hg. This slight change caused 20ml of peroxide to distill from 70-90% in approximately 20 minutes with a loss on the order of 7ml (35% by volume).

It was also found that glassware passivation was very important. Even rinsing in water introduces impurities. These impurities reacted with the peroxide, introducing water and thus

lowering the concentration of the system. Symptoms of

impurities included white foaming during evaporation (not to be

confused with the water boiling out) and a distinct ammonia type

odor of the hot peroxide solution. Distilled water and

isopropyl alcohol must be used on the glassware followed by

passivation with a lower concentration peroxide solution to

'burn' out any impurities.

A 0.5" Lexan shield was constructed to surround the entire

set-up during operation to ensure safety in the unlikely event

of an explosion. Lexan is several hundred times stronger than

Plexiglas. The design of the shield allows the sides to be

removed to gain easy access to all equipment before and after

testing.

In order to determine the particular concentration upon

completion, a hand held refractometer was used. A small drop of

the finished product was placed on the prism and the Brix number

(typically a percentage of solids) was measured. A linear

relationship between Brix number and refractive index exists.

Knowing the refractive index, data from Professor John Rusek at

Purdue University was used to relate it to the HTP

concentration[30]. Figure 19 includes all the relationships to

convert the Brix number to HTP concentration.
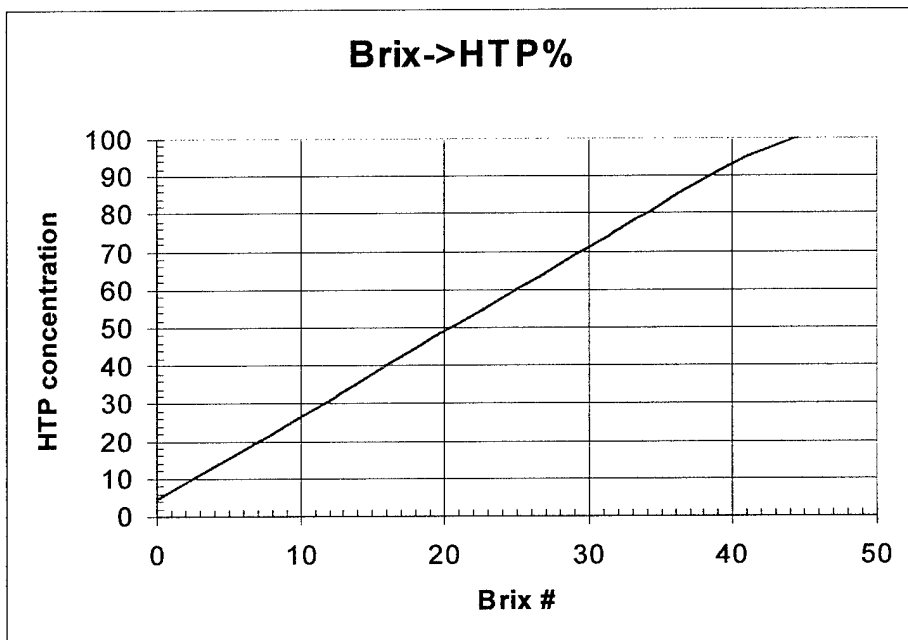
Figure 19. Brix Number to HTP Concentration Conversion

To store the HTP, Polyethylene bottles were purchased with open top PTFE caps. Goretex membrane filters, which allow gas to escape, were used to cover the top to provide the necessary pressure relief. All peroxide was then stored in an explosion-proof chemical storage room.

The results of the numerous distillations can be found in Appendix G. The results show that 30% concentration peroxide proves very infeasible to distill, as losses tend to be on the order of 80% of the volume. The 70% HTP stock, while still having losses of around 40%, can still be distilled effectively on a small scale within a relatively short time frame.

One deficiency of this method of distillation is that stabilizers are left in the peroxide bath. They do not evaporate out with the water. Therefore, knowledge of any other chemical elements in the peroxide solution must be known. MIL-P-16005E lays out the restrictions for impurities. Numerous efforts have been put forth by organizations to meet these specifications. Degussa-Huls comes close to many of these specifications, but still falls short as seen in Table 2 below. The Fisher sample contains much higher amounts of the MIL-SPEC stabilizers plus 6ppm Sodium Stannate, $Na_2Sn(OH_6)$.

	HTP Type I MIL	Degussa "Propulse"
Concentration	90-91	90.0
Chloride	1 max.	2 max.
Ammonium	3 max.	2 max.
Nitrate	3-5 max.	10 max.
Phosphate	0.2 max.	0.5 max.
Sulfate	3 max.	5 max.
Aluminum	0.5 max.	1 max.
Tin	1-4 max.	3-6 max.
Carbon	200 max.	100 max.
Residue of Ignition	20 max.	20 max.
Stability	2% max loss of AO	2% max loss of AO

Table 5:[20] HTP Stabilizer Specifications (all units mg/L)

An alternative method is to concentrate hydrogen peroxide through fractional crystallization. In this method, the solution is chilled until the peroxide begins to freeze. At this point, it is centrifuged out and thawed. The advantage of such a practice is that the impurities tend to stay in the water[50]. Financial constraints did not allow both methods to be pursued so this method was not investigated beyond this point.

5. Modeling

5.1 Micro-Flow

In order to understand the behavior of the fluid in this regime, some basic analysis of the fluid flow was sought. Micro-fluidic simulations are difficult for several reasons, including higher surface effects, a mean free path that is close to the characteristic dimensions, and very low Reynolds numbers. This specific thruster design involves many more complexities in addition to the general ones. It contains a complex three-dimensional flow geometry and combines subsonic and supersonic flow at low Reynolds numbers. The two flow regimes can be seen in Figure 20.
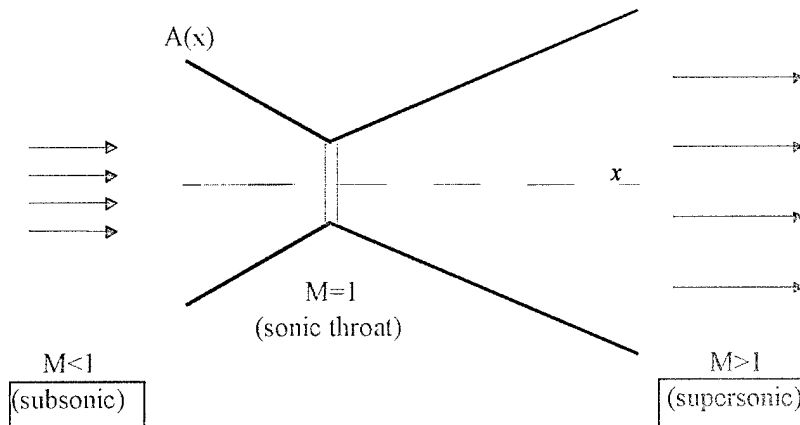
Figure 20. MEMS Nozzle Flow Regimes

Due to the sonic transition at the throat, Mach waves will form, adding more complexity to the problem. Figure 21 models this.
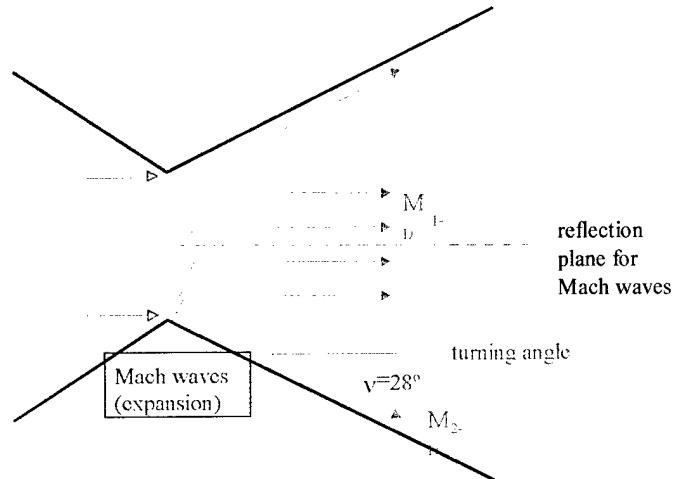
Figure 21. Nozzle Mach Expansion Waves

The result is that with a 28° turning angle, the design that minimizes boundary layers, the local Mach number increases to Mach 2.27. Additional expansion will also occur at the outlet. The result is that a significant amount of the thrust in the axial direction will be diminished in the higher expansion nozzle, as was expected.

Computational Fluid Dynamics (CFD) simulations were initiated to model the flow for performance analysis. As previously mentioned, it is inherently difficult to model combined supersonic and subsonic flows due to the change in character of the partial differential equations (elliptic and hyperbolic). In cooperation with Professor Darren Hitt[51] from the University of Vermont, some one-, two-, and three-dimensional CFD models were constructed using Fluent 5™. The models focused primarily on the nozzle region.

The Fluent 5™ CFD package is a finite volume-based solver with supersonic flow capabilities. Additional effects such as viscous boundary layers, dissipation, and substrate heat transfer were also included. Graphs were created to simulate the flow of non-reacting HTP liquid in the thruster geometry to visualize flow patterns. All simulations assume incompressible flow so there is no choked flow at the nozzle. Fins and filters were neglected to simplify the effort. The flow was set at 390 μg/sec, the desired flow rate. All two and three-dimensional simulations can be found in Appendix H.

Some important initial results were that no vortices or re-circulating flow areas appeared to be present. One possible feature to modify in future designs is the section at the aft end of the catalyst where it narrows down to enter the throat. The angle is set at 45° and it is apparent that a longer transition section may minimize viscous effects entering the throat.

These simulations offer only initial analysis of the flow through a MEMS thruster. Further CFD simulations of the differing designs, including filters and catalyst fins, and reacting and supersonic flow would allow continued optimization of future generations of these thrusters.

5.2 Predicted Results

Before the design was even initialized, estimates of performance parameters were made. As most of this field is in its infancy, it is important to recognize the fact that the degree of accuracy in the estimations was first-order at best. The methods and equations used in analysis were based upon standard combustion and rocket analysis[52]. To begin with, some important chemical properties of HTP were determined. The adiabatic flame temperature of 1400°F was found[25] and verified using the Air Force's ISPcode program. Using the specific impulse (also gained from the ISPcode program) and desired thrust a target mass flow rate can be obtained using:

$$\dot{m} = \frac{F}{I_{SP} g_0} \qquad (8)$$

The mass flow is found to be approximately 390 μg/s for a thrust around 500μN (with no losses). A quick check was determined to see if this flow rate would exceed the flux limitations of a catalyst bed. Typically, flooding occurs when flux exceeds 350 kg/m²s[52]. This thruster is well below that with a flux of 6.5 kg/m²s. The chamber pressure necessary is then determined using:

$$P_0 = \frac{c^* \dot{m}}{A_t} \qquad (9)$$

where c* is a function of the propellant chemistry alone and A_t is the throat area. The exit Mach number is obtained using the nozzle geometry and the propellant chemistry as seen in the implicit equation:

$$\frac{A_e}{A_t} = \frac{1}{M_e}\sqrt{\{\frac{2}{\gamma+1}(1+\frac{\gamma-1}{2}M_e^2)\}^{(\frac{\gamma+1}{\gamma-1})}} \qquad (10)$$

where γ is the ratio of specific heats for the propellant and A_e/A_t is the area of the nozzle exit divided by the nozzle throat (expansion ratio). These calculations as well as others were entered in a Microsoft Excel™ spreadsheet in order to reduce computational effort on multiple design variations. The inputs included the physical design of the thruster, such as the nozzle and catalyst dimensions and the outputs were the theoretical pressures, velocities, impulse, and thrust. An example for design #1 and 90% HTP is shown in Table 6. All quantities in red are user inputs. It is apparent that a 5psi chamber pressure is needed to yield the desired mass flow rate in vacuum conditions. The results yield a specific impulse of 138 seconds and a thrust of approximately 380 μN.

Constants		Design			Outputs		
g	9.81 (m/s^2)				M_c	3.35	
R	8314.41 (J/kmol)				P_e	439.588574 (Pa)	0.063757 (psi)
gamma	1.259	P_a	0 (Pa)	0 (psi)	Expansion	10	
MW	31.241 (kg/kmol)	A_e	0.00000009 (m^2)		c*	794.802375 (m/s)	2607.619 (ft/s)
T_c	1033.15 (K)	A_t	9E-09 (m^2)		P_c	34485.5919 (Pa)	5.001712 (psi)
visc	0.01158 (P)	mdot	3.905E-07 (kg/s)	391 (ug/s)	C_f	1.71074726	
density	1.39 (Mg/m3)	Dt	0.00003 (m)		Isp	138.604076 (s)	
		De	0.0003 (m)		Thrust	0.00053097 (N)	0.000119 (lbf)
		thick	0.0003 (m)		Thrust corr	0.00038229 (N)	8.59E-05 (lbf)
visc(O2)							
visc(H2O-g)		ISPeff	0.8		Re(lqd)	14.3120335	
visc(H2O2)	0.0158	Mdot eff	0.9			2.47151899	
		D_{cat}	0.0002			2.86211218	
		A_{cat}	0.00000006 (m^2)		flux	6.50833333 (kg/m^{2}s)	
flux allowed	250 (kg/m^{2}s)				A_{cat}min	1.562E-09 (m^2)	

Table 6: Expected Performance Characteristics for MEMS
Thruster Design #1

The model is based upon an estimated 80% efficiency in ISP.
This is a result of the fact that some peroxide may make it
through the thruster without even touching the catalyst. A 90%
mass flow rate efficiency is used to account for viscous effects
and low Reynolds numbers[35].

5.3 Trade Studies

Several parameters can be modified in order to optimize the
system, depending on what the mission goals are. If lower
thrusts are required, the chamber pressure can be dropped. One
unique characteristic of this design is that the exit area can
be changed by modifying the etch depth more or less than the
nominal 300 microns. This allows the thrust to change without

modifying the expansion ratio and thus keeping a constant Mach

number.

If high temperatures exceed certain material properties,

the HTP can be diluted to yield lower flame temperatures. For

example, while the 90% concentration has a flame temperature of

1033K, an 80% solution has a flame temperature of 811K.

Performance, however, is degraded as the ISP is lowered by over

5%.

The thrust can be changed by changing the chamber pressure.

However, raising the chamber pressure increases the mass flow

rate. The higher the mass flow rate, the less residence time

the propellant spends in contact with the catalyst. Figure 26

illustrates this for the MEMS design.
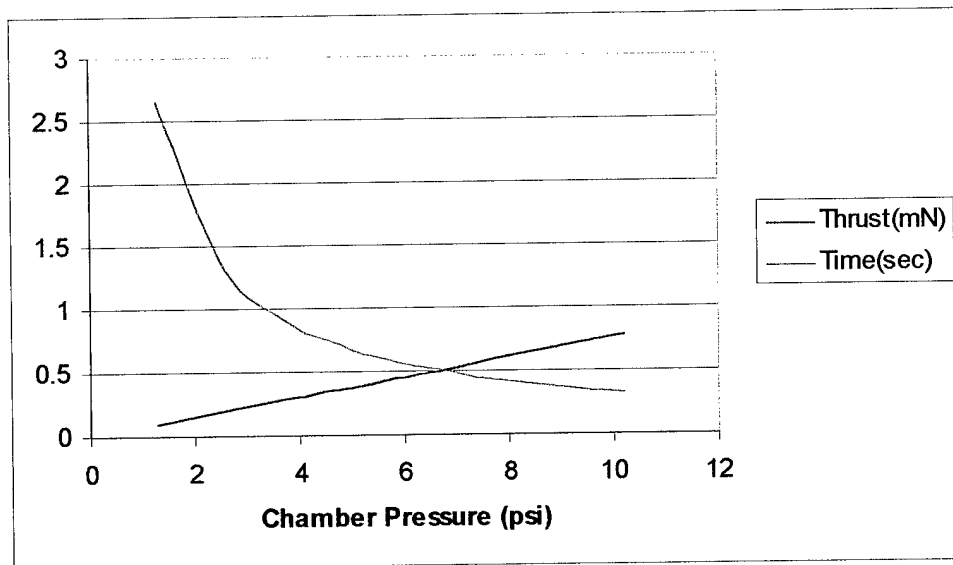
Figure 22. Thrust and Residence Time Tradeoff in Prototype
Thruster

The result is that thrust is not completely dependent on the pressure. Estimations of a required residence time of greater than 0.53 seconds mean that the highest thrust output obtainable is 490μN (corresponding to 6.4psi). Higher pressures and thrust will flood the catalyst, yielding incomplete decomposition.

6. TESTING

6.1 Test Facilities

The NASA Goddard Space Flight Center Advanced Chemistry Laboratory was made available to support the necessary tests. The NASA GSFC Detector Systems Branch provided support for wafer etching, bonding, and dicing. The thrust stand (Figure 27) was built by Dr. Michael Rhee and Dewey Willis of NASA Goddard Space Flight Center. It is a torsional thrust balance which uses laser interferometry to measure the minute displacements expected.
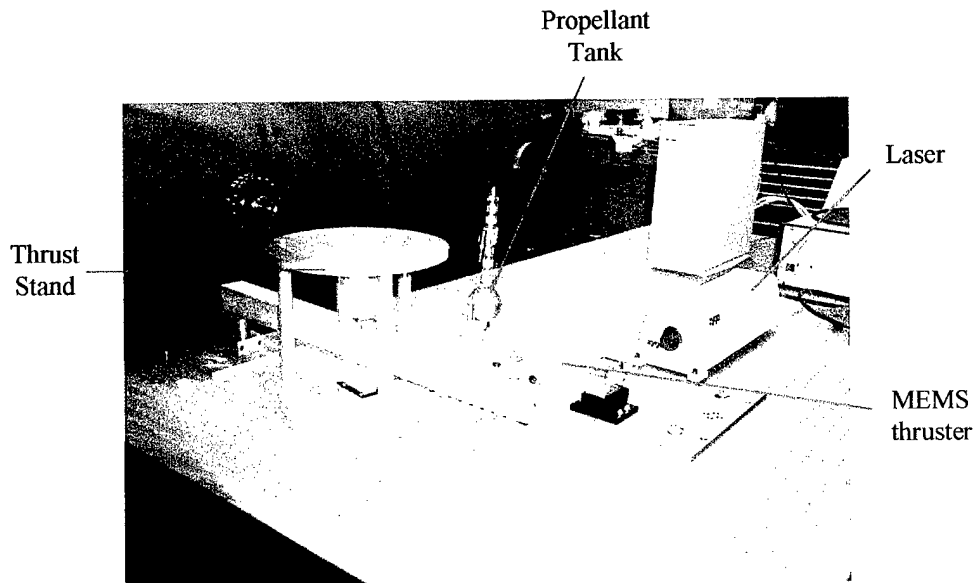
Figure 23. Thrust Stand with MEMS thruster

The thruster is fired in a horizontal direction, normal to the steel beam. The beam will then rotate away from the laser and a linear displacement between the laser and a reflective corner cube will be measured with an interferometer. This

displacement can then be converted into a force. As the arm rotates normal to gravitational acceleration, interference due to gravitational damping is removed, providing access to long or short period oscillations. A magnetic damper helps return the beam to the origin. Calibration was done by timing the period of oscillation and determining the spring constant and moment of inertia of the system. A MatLab model was then created to predict the system response. For a thrust of 300μN, it is expected to see a displacement of 32μm[53].

6.2 Propellant Compatibility

Numerous compatibility tests were run to determine appropriate metals, lubricants, epoxies, and storage containers for the use of hydrogen peroxide as a propellant. The results of these tests can be found in Appendix I. Results confirmed that sufficiently inert materials have been found in all of the aforementioned domains without the requirement of expensive and hard to obtain composite materials.

6.3 Catalyst Reactivity

To aid in the catalyst length verification and understanding, a series of tests was conducted to characterize the reaction of HTP with silver. First, a dimensionless parameter was defined in order to compare the surface area of

99.95% purity silver and the volume of peroxide. Both surface

area and volume were converted to the corresponding radii of a

sphere. The first test involved a ratio of volume to surface

area of 3.92. This was similar to a test documented by Rusek[21].

Using this data and the assumption of a linear reaction

equation, a reactivity constant can be computed from the data as

follows:

$$-\ln \ (Ca/Ca_0)=kt \tag{11}$$

Ca is the peroxide concentration in moles/liter, k is the

1st order reaction constant, and t is time in seconds. The

results, shown below in Figure 28 are consistent with earlier

work. The result is a k value of $5e^{-5}$ for 70% hydrogen peroxide,

which is on the same order of Rusek's experimental value of $2e^{-5}$

for silver oxide, a less reactive catalyst.
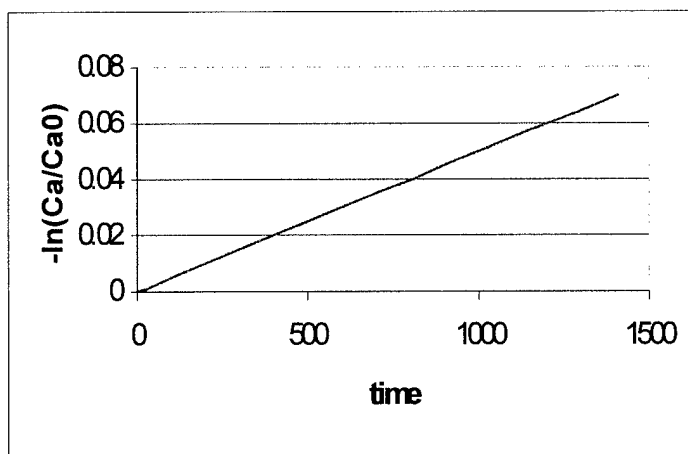
Figure 24. First Order Reaction Constant for HTP
Decomposition Over Time: Ca is HTP concentration and Ca$_0$ is
initial HTP concentration.

Next, smaller ratios were tested. An actual MEMS thruster would have a ratio on the order of 0.5. Test techniques limited the practicality of approaching this ratio, but several ratios were tested to determine a relationship. Figure 29 shows the k value as a function of the surface-area to volume ratio. As expected, lower ratios and higher peroxide concentrations contribute to higher reactivity.

Reactivity/Ratio

- ■ 95%
- ▲ 87%
- ● 70%
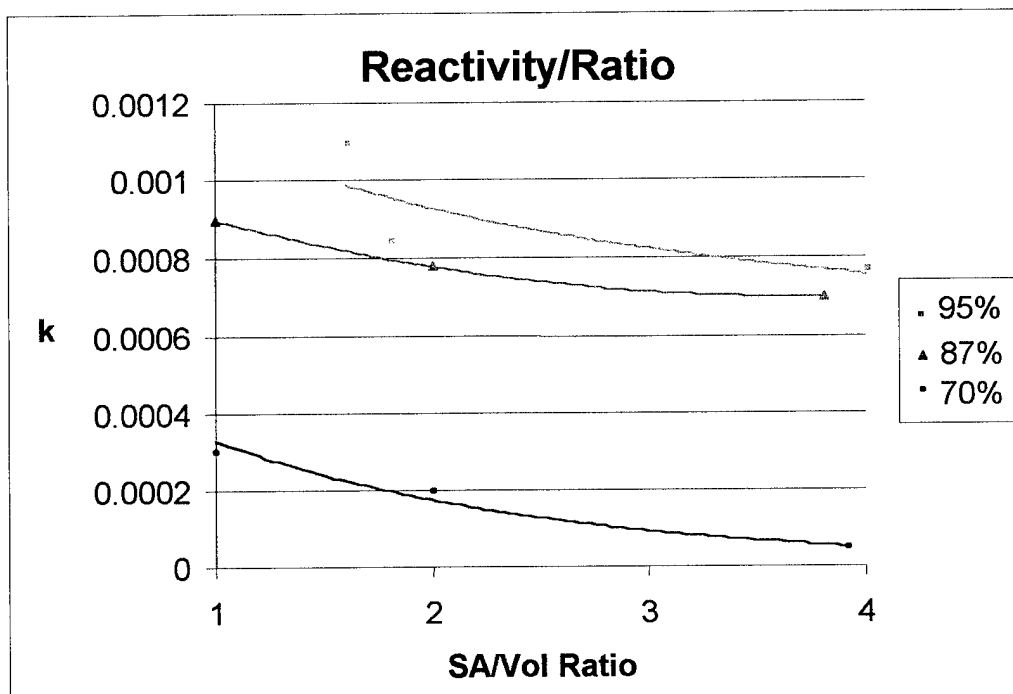
Figure 25. Surface Dependence of HTP-Ag Reaction

Initial analysis shows that the reaction is very temperature dependent. All tests started at 100°F began to rapidly decompose almost instantly. Most of the tests that were started at room temperature slowly reacted until the temperature

71

reached just over 100°F, at which point the reaction rapidly

increased.   However, a few tests at room temperature also

reacted immediately as seen in Figure 30.
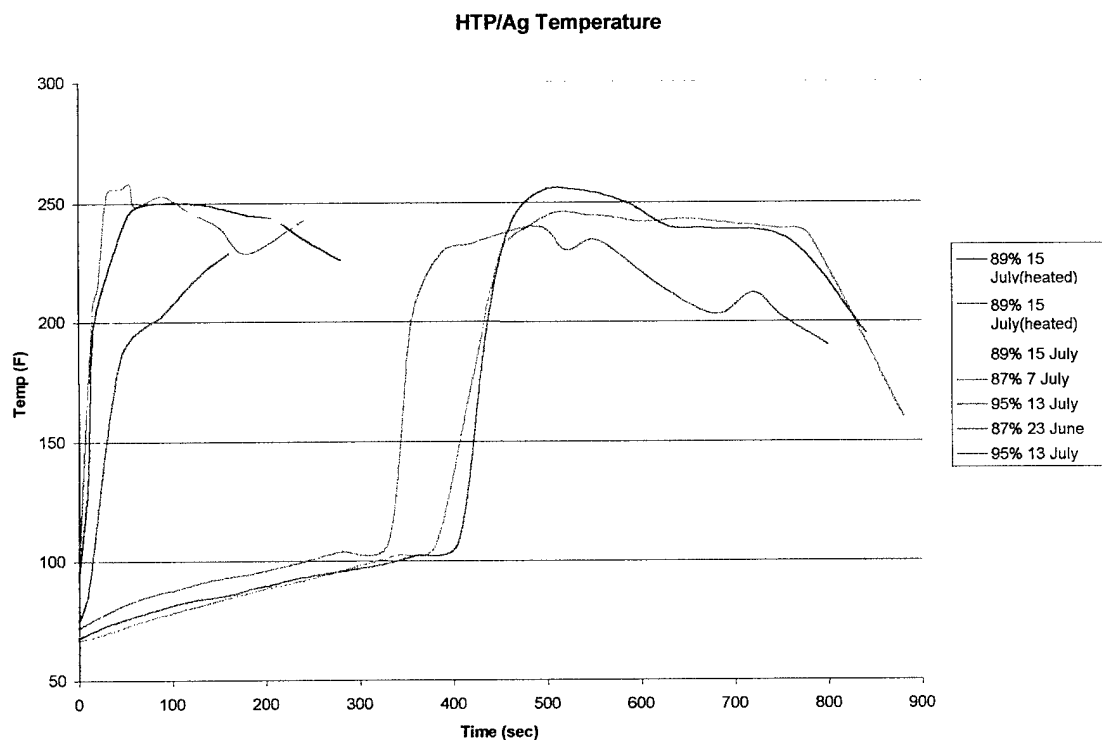
HTP/Ag Temperature

Figure 26: Temperature Data from Ag/HTP tests

The reason for this discrepancy was not immediately

obvious.   Upon further analysis, it was found that a brown layer

was forming over the silver after each test.   Reports from

Whitehead[25] show the formation of brownish-black silver oxide

(Ag_2O) and then gray-black silver peroxide (Ag_2O_2) on catalysts.

Material analysis was performed using an Electron Spectroscopy

for Chemical Analysis (ESCA).   The percentages of elements found

in the sample were found and can be seen in Appendix J.   As

expected, some of this was an oxide layer. The higher

concentration peroxide tests formed silver oxide, while lower

concentrations yielded a layer of silver peroxide. However, a

large amount of phosphorous also appeared to be present.

Phosphorous is used in trace amounts as a stabilizer in HTP

(reference Table 2). Degussa-Huls documents that they use

phosphorous to "be a stabilizer against decomposition caused by

heavy metals[22]."
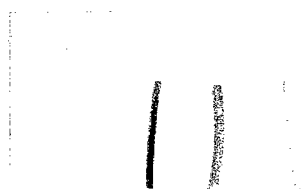
Figure 27: Oxide and Phosphorous Formations on Silver Wire

The data can be explained as follows. At room temperature,

phosphorous began attaching to the active sites of the catalyst,

forming phosphates, and slowing down the reaction. Once it

reached a certain temperature (~110°F), the oxygen from the

phosphates began breaking off, allowing the number of active

sites to increase and the reaction to take off. The pre-heated

batches allowed no time for the phosphorous to form on the

silver. The room temperature tests that took off are a result

of higher purity batches of HTP. Better techniques were used in

the distillation and the original batch contained less initial phosphorous. The HTP, therefore, could react at a lower temperature without phosphorus build-up.

The slow reaction time was a result of the excessive volume to surface area ratio. When used as a propellant, it is desirable that all of the heat of decomposition remain in the system (adiabatic) and vaporize any water present. The large exposed surface area during the tests and the high volume of peroxide removed the heat from the reaction area rapidly.

The maximum temperature reached was around 250°F, which corresponds to the boiling point of 60%HTP. This was the same concentration that most reactions seem to reach thermal equilibrium. The water produced started to evaporate out after 212°F, thus keeping the concentration from changing too rapidly.

The results of these tests validated the k values that were used to design the catalyst lengths. They also helped characterize how the reaction changes with surface area and with temperature. The most helpful result was observing how the reaction is very dependent on the purity of the HTP batch. Great care was then taken to keep the HTP pure for actual thruster firings.

6.4 Test Results

6.4.1 Flow Tests

After sufficient knowledge of the propellant reaction was gained, flow testing on the thruster was initiated. The first tests run on the completed thrusters were flow tests to determine how well they were sealed and whether any internal blockage would prevent propellant from flowing properly. As discussed in Section 4.4, the thrusters were integrated by fitting the chip into a slot cut into the side an aluminum pipe. The top and bottom were then blocked off by epoxy. A Stocker and Yale™ M1000 microscope and Sony Trinitron™ monitor were used to view all operations and a Sony digital camcorder documented most tests.

A water solution containing red dye was used as a referee fluid in the thruster in order to visualize the fluid flow. The results were very promising. No leaks were found in the chip or integration setup, and all channels were free from obstruction. A multitude of flow rates were used from 10-500μg/min. Figure 32 shows the dye in all of the flow passages. Notice the jet that formed outside of the nozzle was much narrower than the nozzle exit. This was expected because of the boundary layer effects.
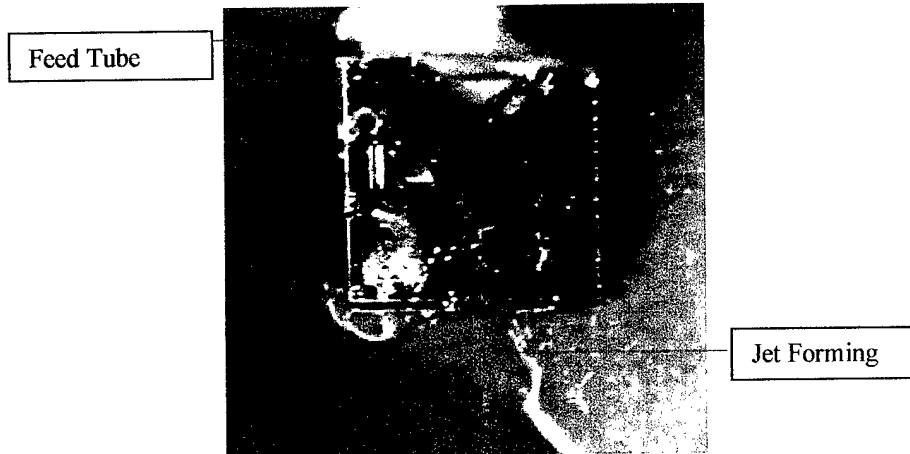
Figure 28. Prototype Thruster Flow Test with Red Dye

After the visualization experiments, hydrogen peroxide was

used in the thruster to determine if appropriate decomposition

occurred. The first batch was 80.5% low purity HTP. Some

decomposition was observed, but some liquid was also exiting the

system indicating that full decomposition was not taking place.

Backflow from the catalyst bed into the plenum was observed as

well. As the peroxide decomposed, large bubbles formed and

pushed omni-directionally. This resulted in liquid and gas flow

through the nozzle as well as back through the filters. This

confirmed the need to incorporate injectors in subsequent

thruster designs.

Additional tests were performed with concentrations of

80.5% to 90% HTP. Most results were very similar to that

previously described. The primary difference was that more

reaction was observed with the higher concentration peroxide

(Figure 33). Using comparisons of liquid peroxide entering the

system with fluid captured after it exited the nozzle, it was seen that 52% of the propellant fully decomposed with a catalyst length of 1mm. The remainder of the liquid had lowered to an average of 70-75% concentration, indicating that evolved water was being carried out of the system. This suggested that the reaction temperature was staying fairly low. The smaller catalysts had percent decompositions under 10% with the exiting peroxide maintaining an 80% concentration. One key observation in these tests was that small flecks of silver were beginning to come loose and discharge though the thruster. Reexamination of earlier thrusters showed that all of the thrusters fired with peroxide had lost large amounts of the silver catalyst.
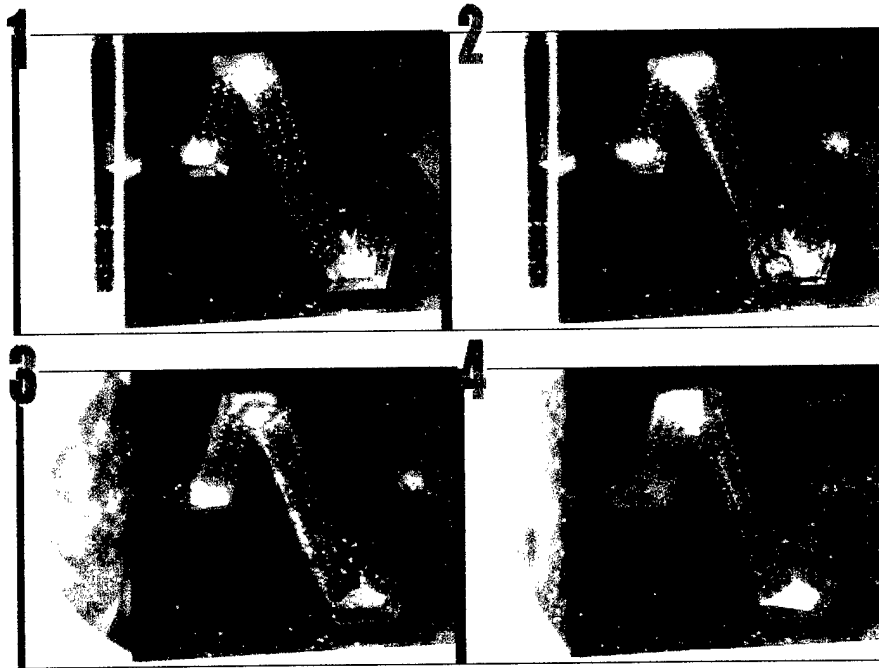
Figure 29. 1st Generation 80% HTP Thruster Firing Sequence
1) Static
2) HTP begins to fill system
3) Gas and liquid pushes out through nozzle
4) Silver begins to flake off and exit

To achieve better decomposition, two options were

considered. Either much longer catalysts needed to be made or

the current ones needed to be optimized. Changing catalyst size

necessitates the creation of a new mask, therefore optimization

was chosen and two improvements were then undertaken. First, a

purge tank was used to keep the oxidation layer from forming on

the silver. Second, a titanium adhesive layer was used to keep

the silver from flaking off. Decomposition tests with the 90%

peroxide were then rerun in several designs of the new set (2nd

generation) of thrusters. Results of the second generation show

that the silver maintains a shiny appearance throughout bonding,

indicating that the purge process was successful in eliminating
oxidation.
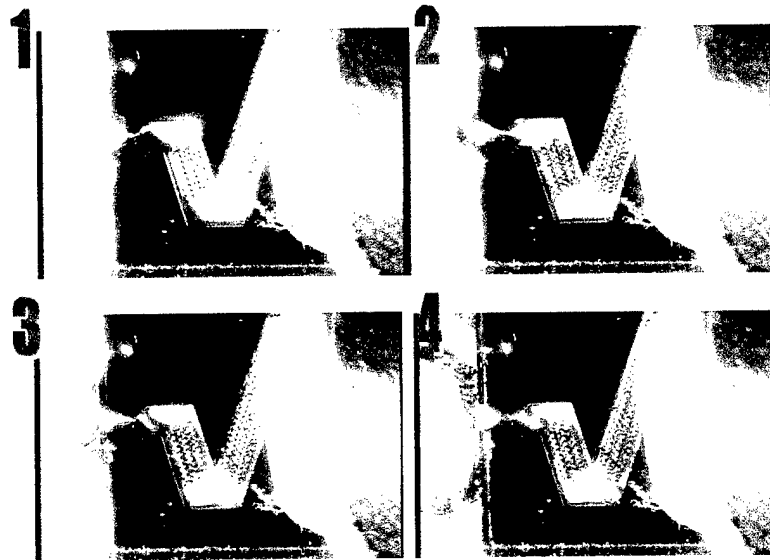
Figure 30. 2nd Generation 90% HTP Thruster Firing Sequence
1)Static
2)HTP fills system
3)Gas pushes out through nozzle
4)Less liquid leaves; no noticeable silver flaking off

The different length catalysts were then all tested in
order to determine the catalyst scaling relationship. The
second generation thrusters were much more reactive (Figure 34).
The 2.5mm catalyst bed only exited 15% liquid. Measuring the
concentration of this product (~70% HTP), it is apparent that
about 3% of the liquid is water that had decomposed but not
evaporated. Also, no silver appeared to flake off throughout
the multiple firings.

The results of the 1st and 2nd generation tests after
correcting for evolved water in the system can be seen in Table
7.

Catalyst Length	1st generation	2nd generation
1mm	32%	71%
1.5mm	55%	77%
2.5mm	63%	88%

Table 7: Average HTP Decomposition Efficiencies in MEMS
Thrusters with Varying Catalyst Lengths

6.4.2 Pressure Tests

Pressure ports were integrated immediately before the feed tube. Attempts were made of validating chamber pressures at the desired flow rates. However, these proved unsuccessful. The auto-decomposition of hydrogen peroxide causes the fluid to constantly maintain small air bubbles. These small air bubbles can carry very large pressure drops across their surface because surface tension forces dominate at this level. While these can be ignored in larger scale systems, the difference is enough at this level to render any sort of a pressure reading grossly inaccurate.

Another issue was that the size of the pressure port was large enough to severely decrease the mass flow until steady-state flow is reached. The large volume required for pressure taps and plumbing make the amount of propellant use and time of firings to be excessive and infeasible. Making valid chamber pressure measurements would require additional effort beyond the scope of this work.

6.4.3 Thrust Tests

The measurement of thrusts at this level requires a unique and specialized thrust stand. The expected thrust output is approximately 300-400μN. Small movements in the system or slight deviations can cause extreme noise when measuring at this level. Therefore, the entire propulsion test system was integrated into an independent board to be placed on the thrust stand. Because some liquid was still exiting the system, steady state flow would have been nearly impossible to observe. Therefore, the system was pulsed at 1-second intervals.

The thruster was designed to operate at vacuum conditions (P_a=0psi). As a vacuum chamber was unavailable for testing, the pressure needed to be controlled at a resolution much lower than the available equipment was able to handle. Hence, the pressures were much higher than required, forcing the mass flow (and flux) beyond the thruster capabilities. The result for design #19 (the largest catalyst) was that nearly pure liquid exited the system. Therefore, thrust stand acquisition equipment read such a high level of noise from the droplets of liquid flowing and dripping that no thrust measurements were capable of being deduced from the readings. Improvements in the pressure feed system are needed in order for valid thrust measurements.

7.Conclusions

7.1 Results Comparison

The MEMS thrusters operated very closely to what was expected. Initial concerns over leakage were assuaged as the system appeared to be very well sealed. Integration to the macro-world is challenging but possible.

While most expected results were met, the main deviation was that large amounts of liquid peroxide were exiting the system in the initial design. In the first generation thrusters, 55% decomposition was found with 90%HTP and a catalyst length of 1.5mm. This obviously falls short of a usable system. As the remaining 45% was exiting at a relatively high concentration, it is logical to conclude that flow paths are either traversing the channels without touching the catalyst-covered walls or that the catalyst is not reactive enough. The second generation containing the titanium adhesive layer and the purged bonding technique produced much more acceptable results. The sudden increase to 88% decomposition shows that the bare silver exhibits much higher reactivity, as expected. These thrusters maintained their catalyst over multiple firings, indicating a reusable thruster manufactured with this technique is possible.

Using the decompositions for multiple lengths, the necessary residence time for 90% hydrogen peroxide in low flow

MEMS thruster appears to be about 0.64 seconds, slightly more than the 0.53 second original baseline calculation. This time corresponds to a length of 4mm for this design. While bordering on being too big for a MEMS thruster, a few things can be done to keep the thruster small. The catalyst can wind around as Design #19 did or the catalyst could be pre-heated with a resistor, allowing shorter lengths. The thrust-weight ratio of the 17mg thruster without a propellant tank is approximately 1.8. Most attitude control thrusters have thrust-to-weights around 0.1[52]. This shows another advantage a MEMS thruster could provide, once valve and tank technology is produced on the MEMS level.

The nozzle design matched expectations and does not produce inhibiting boundary layers at the low flow rates used in these thrusters with the larger divergence angles. The smaller half angles fill with boundary layers and exhibit erratic exiting behavior. The surface tension of the little propellant that does exit inhibits the exiting gasses as it builds up and then pulses, which wreaks havoc in thrust data acquisition.

7.2. Future Generation Design

The next stage of development for the catalytic MEMS thruster is to incorporate the lessons learned from this work into a new generation of thrusters. Several design variables

can be investigated to further optimize the performance of the thruster. With the catalyst length defined, some options for the second-generation design include varying the nozzle dimensions (perhaps the eradication of the nozzle completely), changing the aspect ratio with shallower etchings, and modifying the catalyst into a more curved design to decrease micro-fluidic losses. With use of the Deep Reactive Ion Etcher (DRIE), smaller features and curvatures can be created, increasing the potential for optimized design. An innovative design to incorporate a MEMS injector needs developed. A possible solution could be to do shallower etchings, which would widen the necessary injector width.

Microvalve work remains a missing link in the total development of such a system and work into integrating one into a MEMS thruster is a critical research area. Success would allow multiple thrusters to be built on a single array and pave the way for integration of an independent propulsion system to include tanks, plumbing and reaction bed. These systems could be created on separate wafers and the levels could be bonded together, possibly utilizing the heat of reaction into the valve, and producing a very volume efficient system.

Continued testing of both first and second generation designs is also essential in order to fully characterize the catalyst lifetime and structural degradation. Acquisition of

higher purity peroxide such as Degussa-Huls Propulse™ is another avenue suggested to remove the variability of the propellant purity.

7.3 Implications

The MEMS prototype thruster has validated several key concepts, proving the potential of such a system. While full decomposition was not achieved, enough took place to validate that a MEMS fabricated catalyst is possible at these minuscule lengths and flow rates. The integration of the system has proven that the entire system can be accomplished without insurmountable obstacles.

Innovative techniques are the cornerstone of the aerospace community and the success of technology in America today. MEMS thrusters are a great example of this ingenuity in enabling the use of satellites a mere fraction the size of their predecessors. A catalytic MEMS thruster provides outstanding flexibility in its ability to have variable impulse bits and to have repeatable firings. While prototype thrusters are still under development, the potential results transcend the abilities of nearly every other alternative. Table 8 summarizes the approaches being taken on microthrusters and the advantages that the MEMS catalytic thruster has over each.

Thruster Type	Isp	Thrust uN	Developing Agency	Disadvantage with Respect to MEMS Monopropellant
MEMS Monoprop	160	1-1000	GSFC	
Cold Gas	40-80	500-50000 [0.5]	MIT, JPL, Aerospace	Large Dry and Propellant Mass, Large Volume
Digital Solid	200	[10-100000]	GRC, TRW,CNES	Non-Repeatable Thrust Vector, Limited Total Impulse,
Turbopump	300	$15x10^{\wedge 6}$	MIT, GRC	Very high Minimum Thrust
Digital Bipropellant	200	[3-50]	Princeton, HoneyWell	Non-Repeatable Thrust Vector, Limited Total Impulse.
Resistojet	45-100	[100-1000]	AFRL, USC, Aerospace	Large Power, Lower Specific Impulse Density
Vaporizing Liquid	75-	1-100	JPL	Large Power (1-5W)
FEEP	17000	10-200	SRI, Italy, MSU	Large Dry Mass, Hazardous Propellant
Micro-colloidal	450-1350	20-100	Stanford, MIT	Limited Thrust Range Neutralization Issues
Micro-PPT	800-1000	[0.1-10]	UI, GSFC, EPLI. Primex.	Large power, Large Dry Mass, Limited Thrust Range
Ion Engine	1400-2000	0.1-10	Aerospace Corp. JPL.	Plasma Containment, Electronics Mass. Ion

Table 8: Catalytic MEMS Thruster Comparison to Current Research[16]

As is easily seen, the MEMS catalytic thruster has the potential to be the missing link of microsatellite design. It is very small ($2.75mm^3$), has minimal mass(~17mg), is inexpensive to make and is easily reproducible.

Some of the largest projects in space history are currently underway with the continued development of the International

Space Station and the dreams of a manned mission to Mars.
Meanwhile, some of the smallest projects ever conceived are
quietly pushing the envelope for science and technology.
Ironically, these microscopic miracles may be where the largest
advances of our future may lie.

"There are no small things."

-Bruce Barton

References

1. H. McCurdy, *Inside NASA*, Johns Hopkins University Press, 1993.
2. D. Goldin, Remarks at the FY2001 Budget Press Conference, 7 Feb 2000.
3. J. Pollard, C. Chao, and S. Janson, "Populating and Maintaining Cluster Constellations in Low-Earth Orbit," Proceedings of the 35th AIAA/ASME/SAE/ASEE Joint Propulsion Conference & Exhibit, Los Angeles, CA, June 1999.
4. "Pint-Size Satellites Will Soon Be Doing Giant Jobs," Business Week Online, http://design.caltech.edu/micropropulsion/business_week/index.html, Accessed on 25 May 2000.
5. H. Helvajian, editor, *Microengineering Aerospace Systems*, ISBN 1-884989-03-9, Aerospace Press, El Segundo CA, and AIAA, Reston VA 1999.
6. "MEMS Microthruster Propulsion System," http://www.darpa.mil/MTO/MEMS/Projects/individual_53.html. Accessed on 13 Oct 2000.
7. "Advanced Propulsion Concepts: Micro-thrusters", http://sec353.jpl.nasa.gov/apc/Micropropulsion/01.html. Accessed on 18 Jan 2000.
8. W. Janson and Henry Helvajian, "MEMS, Microengineering, and Aerospace Systems," AIAA 99-3802.
9. M. Zaghoul, "Military Applications of MEMS," George Washington University, http://www.arpa.mil/mto/mems/projects/individual_25.html. Accessed on 5 April 2000.
10. S. Janson, H. Helvajian, W. Hansen, and J. Lodmell, "Batch-Fabricated CW Microthrusters for Kilogram-Class Spacecraft," AIAA 99-2722, Proceedings of the 35th AIAA/ASME/SAE/ASEE Joint Propulsion Conference & Exhibit, Los Angeles, CA, June 1999.
11. R.L. Bayt, A.A. Ayon, and K.S. Breuer, "A Performance Evaluation of MEMS-based Micronozzles," AIAA 97-3169, Proceedings of the 33rd AIAA/ASME/SAE/ASEE Joint Propulsion Conference and Exhibit, Seattle WA, July 1997.
12. B. Reed, "Micropropulsion Activities at NASA Lewis Research Center," Proceedings of the Joint AFRL/MIT Formation Flying and Micro Propulsion Workshop, Oct 1998.
13. E. Antonsson and S.W. Janson, "MEMS Microthruster Digital Propulsion System," Proceedings of the Joint AFRL/MIT Formation Flying and Micro Propulsion Workshop, Oct 1998.
14. D. Lewis, S. Janson, and R. Cohen, "Digital Micro-Propulsion Project," Sensors and Actuators A, 2000. pp. 143-154.
15. G. Spanjers, "Micro-Propulsion Research at Air Force Research Laboratory," Proceedings of the Joint AFRL/MIT Formation Flying and Micro Propulsion Workshop, Oct 1998.
16. C. Zakrzwski, NASA GSFC Propulsion Branch. Private Communication, 2000.
17. M. Giulio, "Design of a Highly Integrated Micropropulsion System for Microsatellites Attitude Control," Proceedings of the 36th AIAA/ASME/SAE/ASEE Joint Propulsion Conference & Exhibit, Huntsville, AL, July 2000.
18. E. Wernimont and P. Mullens, "Capabilities of Hydrogen Peroxide Catalyst Beds," Proceedings of the 36th AIAA/ASME/SAE/ASEE Joint Propulsion Conference & Exhibit, Huntsville, AL, July 2000.
19. "Hazards of Chemical Rockets and Propellants," Chemical Propulsion Information Agency Publication 394, Volume III, Sept 1984.
20. M. Jeff, "Hydrogen Peroxide-The Safe Supply and Handling of HTP," Proceedings of the 1st Annual Hydrogen Peroxide Conference, Surrey U.K. 1998.
21. J.J. Rusek and N.M Anderson, "Heterogeneous Decomposition of Rocket Grade Hydrogen Peroxide," Proceedings of the 1st Annual Hydrogen Peroxide Conference, Surrey, UK, 1998.
22. H.N. Feigenbaum, N. Nimmerfroh, and E. Walzer, "Practical Experiences with High Test Hydrogen Peroxide," Proceedings of the 28th Propellant Development and Characterization Subcommittee and 17th Safety and Environmental Protection Subcommittee Joint Meeting, April 1999.
23. J.C. Whitehead, "Hydrogen Peroxide Propulsion for Smaller Satellites," Proceedings of the 12th AIAA/USU Conference on Small Satellites, SSC98-VIII-1.

24. D. Pauls and S. McMahon, "Transportation, Storage and Handling of PROPULSE™ HTP," Proceedings of the 2nd International Hydrogen Peroxide Conference, Nov 1999.

25. J.C. Whitehead, "Hydrogen Peroxide Propulsion for Smaller Satellites," Proceedings of the 12th AIAA/USU Conference on Small Satellites, SSC98-VIII-1.

26. 25. M.K. Minthorn, "Future Navy Missile Propulsion Needs," Proceedings of the 2nd International Hydrogen Peroxide Conference, Nov 1999.

27. E.J. Wernimott, M. Ventura, G. Garboden, and P. Muellens, "Past and Present Uses of Rocket Grade Hydrogen Peroxide," Proceedings of the 2nd International Hydrogen Peroxide Conference, Nov 1999.

28. "TSRS MSDS Number 08193," http://msds.ksc.nsaa.gov/msds/08192.html Accessed on 5 Feb 2000.

29. J. McCormick, "Hydrogen Peroxide Rocket Manual," FMC Corporation.

30. "Hydrogen Peroxide for Rocket Propulsion Applications," J. Rusek, Chemical Propulsion Information Agency Publication 630, Volume I, Dec 1995.

31. "Hazards of Chemical Rockets and Propellants," Chemical Propulsion Information Agency Publication 394, Volume III, Sept 1984.

32. J.C. Whitehead, "Progress Towards Hydrogen Peroxide," Proceedings of the 13th AIAA/USU Conference on Small Satellites, SSC98-XII-5.

33. Chemical Propulsion Information Agency, Liquid Propellant Manual, September 1997.

34. N. Nimmerfroh, H. Feigenbaum, and E. Walzer, "PROPULSE™ Hydrogen Peroxide: History, Manufacture, Quality, and Toxicity," Proceedings of the 2nd International Hydrogen Peroxide Conference, Nov 1999.

35. D.R. Mattie, "Toxicity of Rocket Fuels: Comparison of Hydrogen Peroxide with Current Propellants," Proceedings of the 1st Annual Hydrogen Peroxide Conference, Surrey, UK, 1998.

36. E.J. Wernimott, M. Ventura, G. Garboden, and P. Muellens, "Past and Present Uses of Rocket Grade Hydrogen Peroxide," Proceedings of the 2nd International Hydrogen Peroxide Conference, Nov 1999.

37. M.K. Minthorn, "Future Navy Missile Propulsion Needs," Proceedings of the 2nd International Hydrogen Peroxide Conference, Nov 1999.

38. Proceedings of the 2nd International Hydrogen Peroxide Conference, Nov 1999.

39. J. Mueller, J. Bellan, F. Noca, and I. Chakraborty, "Feasibility Investigation of a Microfabricated Vaporizing Liquid Micro-Thruster," JPL Proposal , 21 January 1999.

40. "Catalysis," http://www.chem.ualberta.ca/~plambeck/che/p102/p02173 Accessed on 8 April 2000.

41. R. Eloirdi, S. Rossignol,M. Chauveau,C. Kappenstein, and D. Duprez, "Design and Use of a Batch Reactor for Catalytic Decomposition of Different Monopropellants," Proceedings of the 36th AIAA/ASME/SAE/ASEE Joint Propulsion Conference & Exhibit, Huntsville, AL, July 2000.

42. J.J. Sellers, R. Brown, and M. Paul, "Practical Experience with Hydrogen Peroxide Catalysts," Proceedings of the 1st Annual Hydrogen Peroxide Conference, Surrey, UK, 1998.

43. J. Rusek, Professor at Purdue University. Private Communication, Oct 1999.

44. M. Bettner and R. Humble, "Polyethylene and Hydrogen Peroxide Hybrid Testing at the United States Air Force Academy," Proceedings of the 1st Annual Hydrogen Peroxide Conference, Surrey U.K. 1998.

45. W. Janson and Henry Helvajian, "MEMS, Microengineering, and Aerospace Systems," AIAA paper 99-3802, 1999.

46. R.L. Bayt, A.A. Ayon, and K.S. Breuer, "A Performance Evaluation of MEMS-based Micronozzles," Proceedings of the 33rd AIAA/ASME/SAE/ASEE Joint Propulsion Conference and Exhibit, Seattle WA, July 1997, AIAA paper 97-3169.

47. P.V. Panetta, "NASA-GSFC Nano-Satellite Technology Development," Proceeding of the 12th AIAA/USU Conference on Small Satellites, SSC98-VI-5.

48. "Advanced Propulsion Concepts: Micro-Thrusters," http://sec353.jpl.nasa.gov/apc/Micropropulsion/01.html. Accessed on 18 Jan 2000.

49. B. Mott, NASA GSFC Detector Systems Branch. Private Communication, Jan 2000.

50. J. Whitehead, "Hydrogen Peroxide Storage in Small Sealed Tanks," Proceedings of the 2nd International Hydrogen Peroxide Conference, Nov 1999.

51. D. Hitt, University of Vermont. Private Communication, Aug 2000.

52. R. Humble, *Space Propulsion Analysis and Design*, McGraw-Hill. 1995.

53. D. Willis, NASA GSFC Propulsion Branch. Private Communication, Oct 2000.

Appendix A: Hydrogen Peroxide Chemical Properties

PROPERTY	ENGLISH UNITS	SI UNITS
Boiling Point	286.1°F	414.3K
Freezing Point	11.3°F	261.65K
Density(Liquid)	11.5lb/gal @68°F	1.390 Mg/m^3 @293K
Vapor Pressure	0.05psia @68°F	0.345kPa @293K
	0.17psia @104°F	1.17kPa @313K
	0.52psia @140°F	3.59kPa @333K
	1.38psia @176°F	9.52kPa @353K
Coefficient of Viscosity Kinematic: Absolute:	0.905 centistokes@68°F 1.26 centistokes@68°F	9.05×10^{-7} m2/s@293K 1.26×10^{-3}Pa s @ 293 K
Explosive Range	26-100% by volume in air	
Flammability Limit Lower: Upper:	26 volume %hydrogen peroxide in air 100 volume %hydrogen peroxide in air	

Table A-1: Selected Chemical Properties of Hydrogen Peroxide[19]

Appendix B: Hydrogen Peroxide First-Aid

The first aid procedures for exposure are:

Eyes:
    Tilt Head Back and rotate affected eye toward ground. Immediately flush with large amounts of clean water for at least 15 minutes. Pour from nose side outward to keep other eye from being exposed and occasionally lift the upper and lower eyelids. Rinse the surrounding face and other exposed areas well, including the scalp, seternal ear and canal. Patch the eye to keep the patient from rubbing eye. Call hospital immediately.

Skin:
    Remove all contaminated Clothing and Wash all exposed Skin Immediately with water for at least 15 minutes. A mild (non-abrasive) soap with the water may be used. Call hospital immediately.

Ingestion:
    If patient is awake and alert:
Immediately drink large quantities of water. Do not induce vomiting. Have patient Rinse mouth. Call hospital immediately.

    If patient is unresponsive:
Check for spinal cord injuries, turn the patient's head to ensure he does not aspirate if he vomits. Call hospital immediately. Wash exposed skin with mild (non-abrasive) soap and water.

Inhalation

    If person experiences nausea, headache or dizziness, person should stop work immediately and move to fresh air until these symptoms disappear. Call hospital immediately.
    If a person loses consciousness, person should be moved to fresh air at once. Call hospital immediately.

Spill Response

In the event of spill immediate attention should be given to any injuries and limiting the spread of the spill. An assessment should be made of the size of the spill. Because a spill may represent an explosive hazard if HTP is in contact with various metals, any metals which may have been accidentally placed in the path of the spill must be removed. All sources of ignition must be removed.

Dilution with water renders HTP harmless, therefore copious amounts of water should be applied to any surfaces contaminated or in imminent contact. Sorbent pads should be placed on the spilled HTP. Clean up using an "outside-in" approach (outside edges will be cleaned up, working inward). The containment sorbent and other expendable materials should be placed in the spill response container. The area should be washed/wiped twice with a mild detergent and water using mop, sponge, and cloths specifically designated for spill clean up. Rinse area with water and dry the area with rags and cloths. Contain any materials used during the cleanup and decontamination in the spill response container and flush with water.

Appendix C: HTP Compatibility Tables

Stainless Steels	Class	Plastics	Class
302	2	Tygon 360A	2
304	2	Vicone	2
310	2	Vinyl 29139	2
316	2	Vinylite VU1940	3
316 porous	4	Viton A(271-7)(770545)	2
329	3	Viton A(V271-7)	4
347	2	Viton B 805	3
AM355	3	Lubricants	
410	4	Arochlo 1221	4
416	4	Bardahl	4
420	4	Ceresin Wax	4
440	4	Fluorlube FS	2
440C	3	Fluorolube Heavy Grease	2
17-7PH, 37-45Rc	2	Halocarbon Light Oil 11-21	2
Durimet 20	3	Kel-F Alkane	2
		Kel-F Light Oil No. 1	2
Plastics		Mineral Oil	4
Aclar	1	LubriSeal	4
Acrylon rubber BA-12	4	Petrolatum	4
Bisolin No. 50	2	Silicone Oil DC-7	4
Buna N	4	Tributyl Phosphate	4
Fluorel 2141	3	Miscellaneous	
Fluorosilicone LS-53	2	Al-Si-Mag Porcelain	2
GE 12601	4	Aluminum silicate	2
GE 12650	2	Alundum La 116	2
Geon 404	3	Boron Nitride	4
Halgene	2	Carbaloy	4
Hypalon S-2	4	Ceramic AB-2	2
Kel F	1	Ceramic AL-200	2
Kel-F800	1	Graphite	4
Mylar A	1	Karbate	4
Nylon	4	KT Silicon Carbide	2
Phenol-formaldehyde	4	Norbide	2
Plexiglas	4	Pyroceram	1
Polyethylene	2	Synthetic sapphire	1
Polystyrene	2	Zirconium silicate	2
Saran	2		
Silastic 152	3		
Silastic 9711	2		
Silicone 407-B-217-1	3		
Silicone Y-1749	2		
Polytetrafluoroethylene, TFE	1		

Table C-1: Compatibility of Selected Materials with HTP

*Class 1: No reaction; can be used for storage
*Class 2: Slight reaction; can be used for short-term contact
*Class 3: Not recommended for use
*Class 4: Violent Reaction

Appendix D: Catalyst Surface Area Calculations

*All Designs Depicted in Figure 7

<u>Design A:</u>

Each diag= $2*141.4*10^{-6}*300*10^{-6} = 8.48*10^{-8}$
Entire zag= $7*8.48*10^{-8} = 5.9388*10^{-8}$
Each side= $750*10^{-6}*300*10^{-6} = 2.25*10^{-7}$
Total=Entire zag+2*Each side= $5.9388*10^{-8} + 2*2.25*10^{-7} = \mathbf{5.093*10^{-7}m^2}$

<u>Design B:</u>

Each strip= $750*10^{-6}*300*10^{-6}*2 = 4.5*10^{-7}m^2$
Total=3*Each strip+2*Each side= $3*4.5*10^{-7}m^2 + 2*2.25*10^{-7} = \mathbf{1.80*10^{-6}m^2}$

<u>Design C:</u>

Each diag= $42.42^{*}10^{-6}*300*10^{-6} = 1.27*10^{-8}$
Each strip= $23*Each diag*2 = 5.85*10^{-7}$
Total=3*Each strip+2*Each side= $3*5.85*10^{-7} + 2*2.25*10^{-7} = \mathbf{2.206*10^{-6}m^2}$

<u>Design D:</u>

Each block= $30*10^{-6}*4*300*10^{-6} = 3.6*10^{-8}m^2$
Total=40*Each block+2*Each Side= $1.44*10^{-6}m^2 = \mathbf{1.89*10^{-6}m^2}$

Appendix E: Catalyst Length Baseline Calculations

Air Force Academy Catalyst:

L=3"=0.0762m
Mass flow rate=0.4 kg/sec
Catalyst Frontal Surface Area=0.002m^2
ρ_{HTP}=1.29Mg/m^3=1290kg/m^3

*Use fact that velocity is equivalent to the mass flow rate divided by the area and the density. Then notice that the residence time is the catalyst length divided by the velocity (dimensional analysis can be used to verify).

$$v = \frac{\dot{m}}{A\rho} = 0.4 \frac{kg}{\sec} * \frac{1}{0.002m^2} * \frac{1m^3}{1390kg} = 0.144 \frac{m}{s}$$

$$t = \frac{L}{v} = \frac{0.0762m}{0.144\frac{m}{s}} = 0.53 \sec$$

MEMS prototype thruster:

Mass Flow Rate= 390ug/sec
Catalyst Frontal Surface Area=7.8*10^{-8} m^2
ρ_{HTP}=1.39Mg/m^3=1390kg/m^3

$$v = 390*10^{-9} \frac{kg}{\sec} * \frac{1}{7.8*10^{-8}m^2} * \frac{1m^3}{1390kg} = 0.003 \frac{m}{s}$$

$$t = 0.53\sec = L/v => L = 0.53\sec * 0.003\frac{m}{s} = 1700\mu m$$
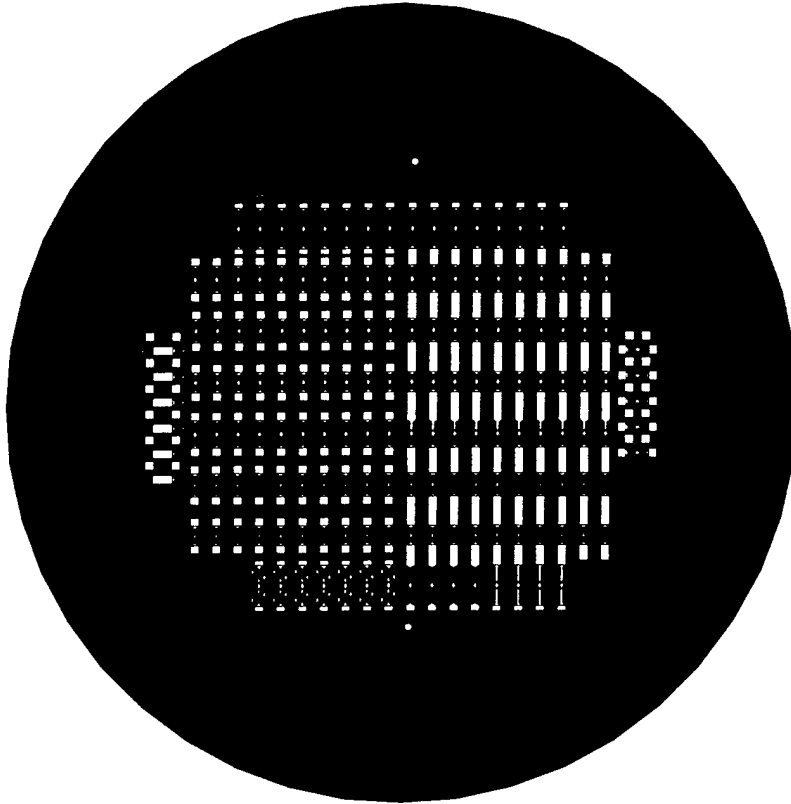
Appendix F: MEMS Mask Layout

Figure F-1: Mask Design for MEMS Thrusters

*Small dimensional size makes it difficult to see details without a wall-size poster blow-up of above figure.

Appendix G: Distillation Data

	Test #1	Test #2	Test #3	Test #4	Test #5	Test #6	Test #7	Test #8	Test #9
Initial Concentration:	70%	70%	70%	70%	30%	70%	30%	70%	70%
Initial Volume:	27ml	27ml	50ml	40ml	70ml	60ml	100ml	80ml	20ml
Stock:	D-Huls	D-Huls	D-Huls	D-Huls	Fischer	D-Huls	Fischer	D-Huls	D-Huls
Elapsed Time:	120 min	90 min	30min	20min	45min	30min	35min	15min	15min
Vacuum Achieved:	25"Hg	27"Hg	24.5"Hg	28"Hg	26"Hg	27"Hg	27"Hg	27"Hg	27"Hg
Final Concentration	81%	87%	70%	90%	89%	96%	91%	89%	87%
Final Volume:	15ml	20ml	40ml	28ml	15ml	25ml	20ml	42ml	12ml
Volume Lost:	44%	26%	20%	30%	78%	58%	80%	48%	40%

Average Loss from 30%:   79%
Average Loss from 70%:   38%

*Test #3 had contamination

Table G-1: Distillation Data for Hydrogen Peroxide

Appendix H: CFD Simulations

*All Simulations were done by Professor Darren Hitt[51]. All represent non-reactive flow of 90%hydrogen peroxide at 390 ug/s, a chamber pressure of 5 psia and atmospheric pressure of 0 psia. Thruster geometry is modeled after Thruster ID#1 (see Table #4).
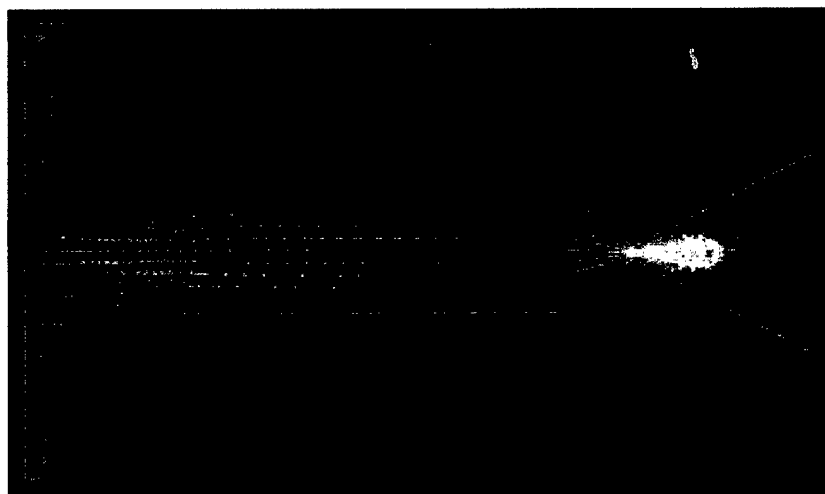

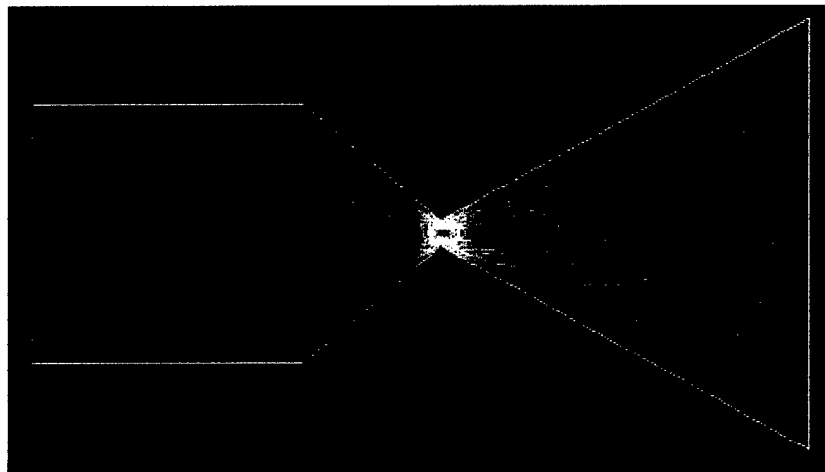Figure H-1: 2-D CFD Subsonic Velocity Field Results in MEMS Thruster
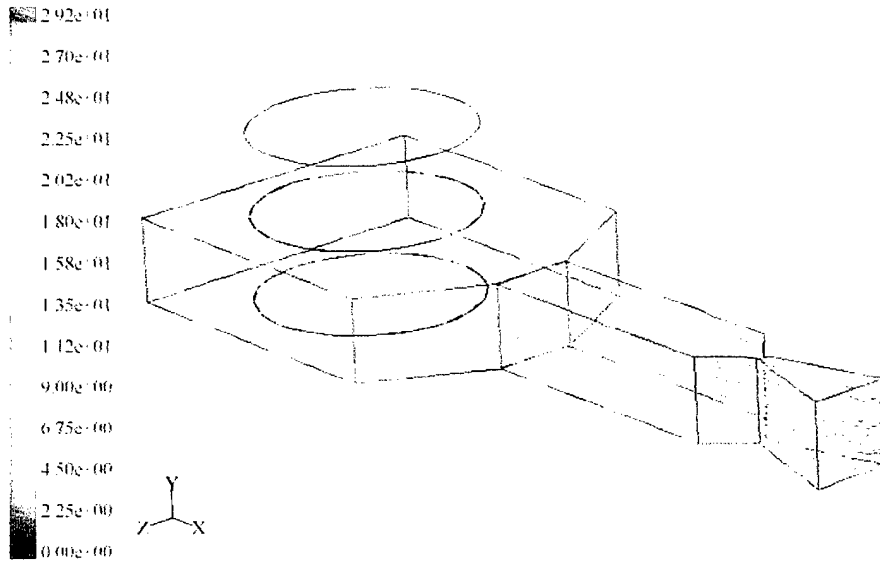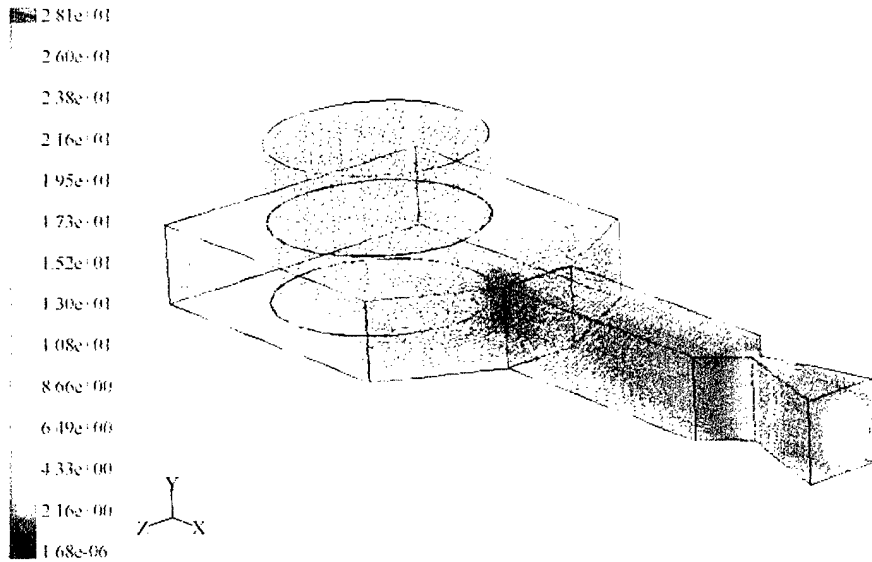

Figure H-2: 2-D CFD Nozzle Velocity Contours for MEMS Thruster Nozzle

Figure H-3: 3-D Subsonic CFD Streamlines

Rel Velocity Vectors Colored By Velocity Magnitude (m/s)

Figure H-4: 3-D Subsonic CFD Velocity Vector Plot

Appendix I: Specific Compatibility Data

Material:	Class:	Reaction Notes:	Potential Use:
Aluminum 1100	1	-no effect	Plumbing/ Tanks
Aluminum 6061	3	-HTP bubbling, material tarnished	Plumbing/ Tanks
Brass	2	-HTP bubbling, no permanent material effect	Plumbing
Ceramic (rough)	2	-rough ceramic formed crust	MEMS holder
Ceramic (smooth)	1	-no effect	MEMS holder
Copper	2	-slight bubbling and tarnished	Plumbing
Colored Dyes	1	-no effect	Flow Testing
Diamond Powder	1	-no effect	Drill Residue
Iron	3	-moderate bubbling, crusting	Plumbing
Isopropyl Alcohol	1	-slowed down reaction through dilution	Cleaning
Lexan	1	-no effect	Cover Slip
Nickel	2	-HTP bubbling, tarnished	Plumbing
Nitrile	1	-no effect	Seals/PPE
Polyethylene HD	1	-no effect	Tanks
Polyethylene LD	3	-melting	Tanks
Pyrex 7740	1	-no effect	Cover Slip
Stainless Steel 316	1	-no effect	Plumbing
Teflon	1	-no effect	Seals

Table I-1: Hydrogen Peroxide Compatibility Data with MEMS Specific Materials

Electron Spectroscopy for Chemical Analysis(ESCA)

```
Thu Aug 83 11:28:26         M-Probe ESCA Console        User ID: HST
W02602A.MRS       Thu Aug 83 18:53:28 2888   Operator: pai
silver wire test 1a 70% sputtered
Spot:        600µ         Resolution:       3    Energy:
Scans:    4 of   4        Neutralizer:    Off    Counts:
Region:      1/  2        Aperture:      None
```
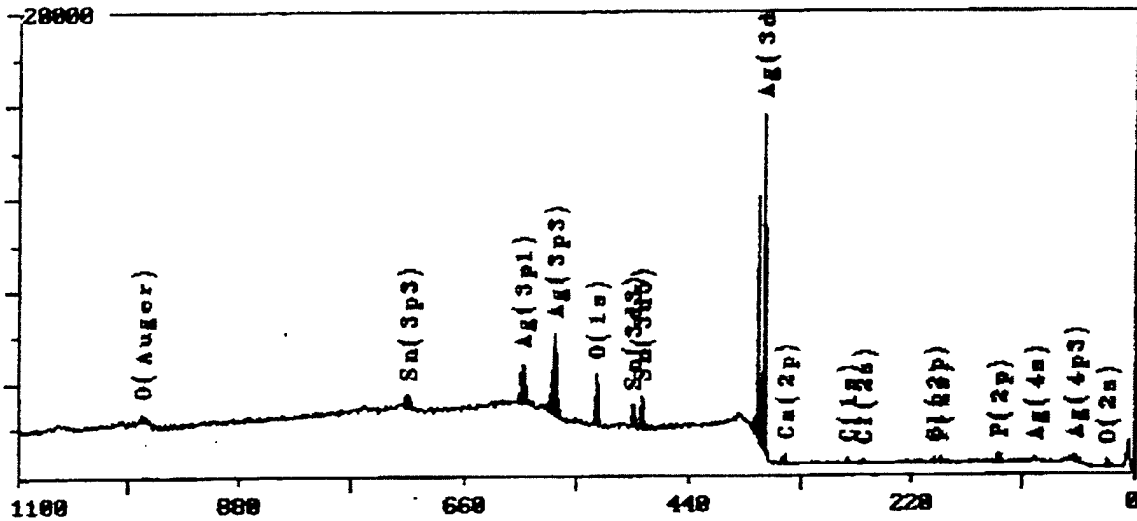

Surface Composition Table Summary

File name: WO2602A.MRS
Region: 1
Description: silver wire test 1a 70% sputtered

Operator: pai
Date: Thu Aug 3 10:53 2000

Element	Binding Energy	atom %
O (1s)	531.5	35.39
Sn (3d5)	487.2	3.21
Ag (3d)	368.4	36.25
Ca (2p)	347.6	3.12
C (1s)	284.6	7.26
Cl (2s)	269.2	3.75
P (2p)	134.1	11.03

Figure J-1: ESCA Analysis of 70%HTP Applied to Silver Wire

Thu Aug 03 13:23:54   M-Probe ESCA Console   User ID: HSI
W02603A.MRS   Thu Aug 03 13:22:07 2000   Operator: pai
silver wire test 1b 90% sputtered
Spot: 600µ   Resolution: 3   Energy:
Scans: 4 of   4   Neutralizer: Off   Counts:
Region: 1/ 2   Aperture: None
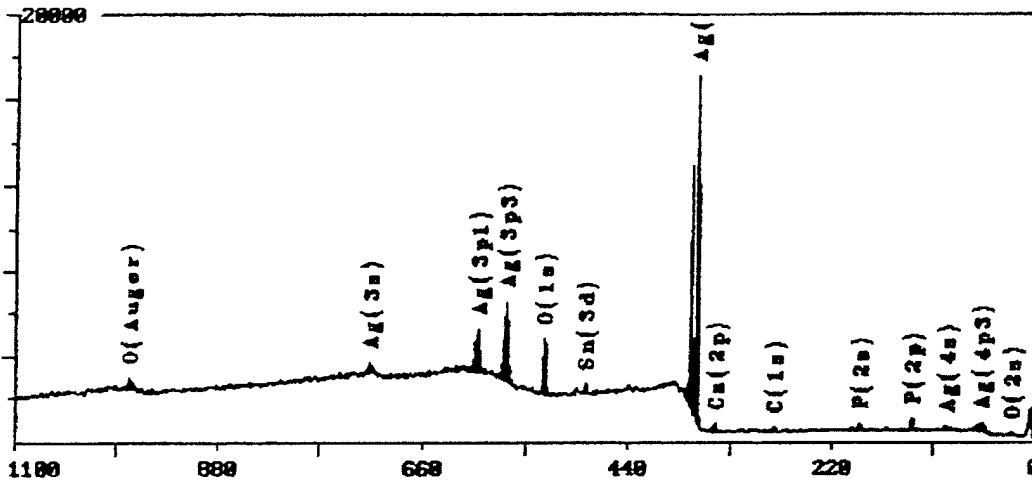
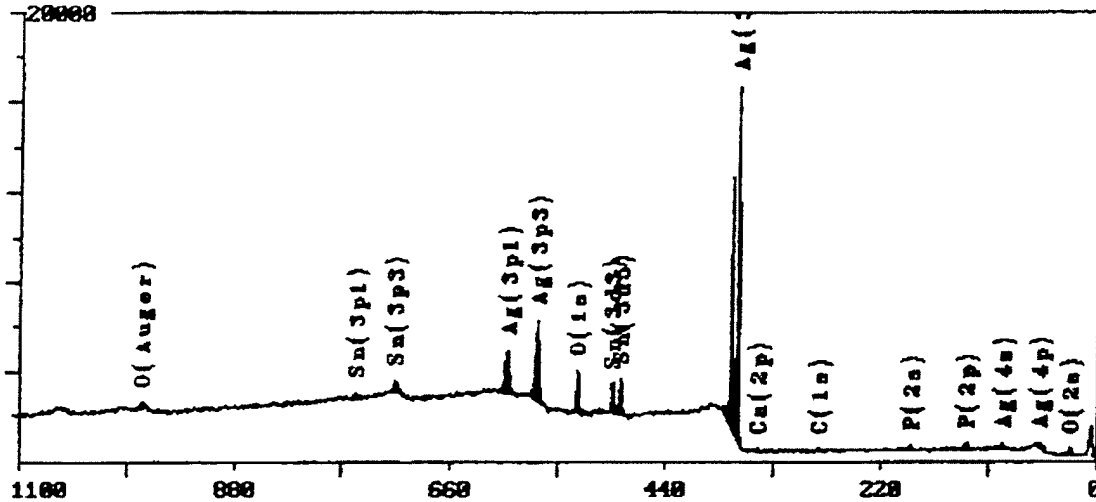**Surface Composition Table Summary**

File name: WO2603A.MRS
Region: 1
Description: silver wire test 1b 90% sputtered

Operator: pai
Date: Thu Aug 3 13:22 2000

Element	Binding Energy	atom %
O (1s)	531.5	40.53
Sn (3d)	487.4	0.48
Ag (3d)	368.4	36.61
Ca (2p)	347.6	3.27
C (1s)	284.6	6.32
P (2p)	134.1	12.79

Figure J-2: ESCA Analysis of Low-Purity 90%HTP Applied to Silver Wire

Thu Aug 03 13:58:59   M-Probe ESCA Console   User ID: HST
W02604A.MRS   Thu Aug 03 13:37:38 2000   Operator: pai
silver wire test 2b 90 from 70% sputtered
Spot: 600µ   Resolution: 3   Energy:
Scans: 4 of   4   Neutralizer: Off   Counts:
Region: 1/   2   Aperture: None

Surface Composition Table Summary

File name: W02604A.MRS
Region: 1
Description: silver wire test 2b 90 from 70% sputtered

Operator: pai
Date: Thu Aug 3 13:37 2000

Element	Binding Energy	atom %
O (1s)	531.2	35.06
Sn (3d5)	487.0	4.13
Ag (3d)	368.2	43.39
Ca (2p)	347.2	0.81
C (1s)	284.6	6.27
P (2p)	133.7	10.34

Figure J-3: ESCA Analysis of 90%HTP Applied to Silver Wire

Thu Aug 03 10:37:21   M-Probe ESCA Console   User ID: HST
W02601B.MRS   Thu Aug 03 10:19:40 2000   Operator: pai
silver wire sputtered
Spot: 600μ   Resolution: 3   Energy:
Scans: 4 of   4   Neutralizer: Off   Counts:
Region: 1/   2   Aperture: None
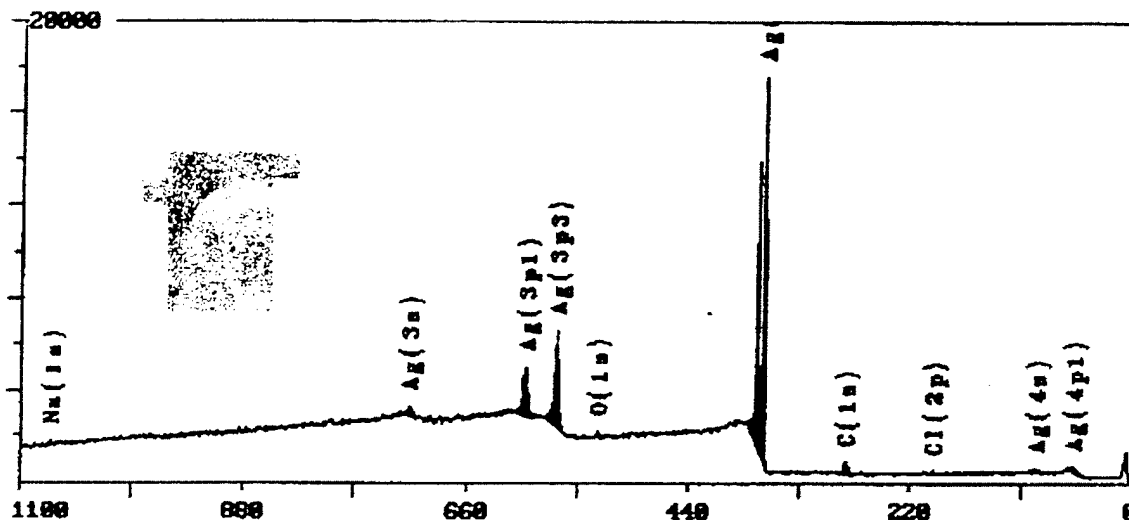
Surface Composition Table Summary

File name: W02601B.MRS
Region: 1
Description: silver wire sputtered

Operator: pai
Date: Thu Aug 3 10:19 2000

Element	Binding Energy	atom %
Na (1s)	1071.3	2.61
O (1s)	531.2	5.74
Ag (3d)	367.9	59.82
C (1s)	284.6	29.17
Cl (2p)	198.0	2.66

Figure J-4: ESCA Analysis Bare Silver Wire